Tucholke, B.E., Sibuet, J.-C., and Klaus, A. (Eds.)
Proceedings of the Ocean Drilling Program, Scientific Results Volume 210

14. Linking Core and Seismic Data without Logs: Core-Seismic Correlation at Site 1276[1]

Donna J. Shillington,[2] Brian E. Tucholke,[3] Garry D. Karner,[4,5] Dale S. Sawyer,[6] W. Steven Holbrook,[7] and Heike Delius[8]

ABSTRACT

Forging a link between seismic data and the 936.9 m of core data at Ocean Drilling Program Site 1276 is essential to understand the tectonic and sedimentary history of the wider Newfoundland Basin. Logging data traditionally bridge the gap between core and seismic data by measuring in situ geophysical properties of borehole lithologies at a scale intermediate between seismic and core data. Unfortunately, such data could not be collected at Site 1276 because of unstable hole conditions. In lieu of logging data, we employed shipboard laboratory measurements of density and velocity to create synthetic seismograms in order to tie seismic data to core data at Site 1276. The upper 800 m of sediment at Site 1276 were not cored or logged. To establish a link between the top of the cored section and two-way traveltime, we determined velocities in the upper 800 m by analyzing multichannel seismic reflection data and refined the link by comparing the reflection characteristics of seismic data and synthetic seismograms beneath 800 meters below seafloor. We demonstrate that the prominent U reflection, which is observed throughout much of the Newfoundland Basin, is at least locally created by the shallower of two postrift igneous sills encountered at the base of Site 1276. A brighter reflection that lies beneath the U reflection is generated by the strong impedance contrast between very low-velocity, low-density sediments (interpreted as undercompacted) and the deeper postrift sill. Additionally, we describe linkages between other seismic stratigraphic horizons, such as Horizon A^U, and the boundaries between primary lithologic units in Site 1276.

[1]Shillington, D.J., Tucholke, B.E., Karner, G.D., Sawyer, D.S., Holbrook, W.S., and Delius, H., 2007. Linking core and seismic data without logs: core-seismic correlation at Site 1276. *In* Tucholke, B.E., Sibuet, J.-C., and Klaus, A. (Eds.), *Proc. ODP, Sci. Results,* 210: College Station, TX (Ocean Drilling Program), 1–33. doi:10.2973/odp.proc.sr.210.110.2007
[2]National Oceanography Centre, Southampton, University of Southampton, School of Ocean and Earth Science, European Way, Southampton SO14 3ZH, United Kingdom. **djshill@noc.soton.ac.uk**
[3]Department of Geology and Geophysics, Woods Hole Oceanographic Institution, Woods Hole MA 02543-1541, USA.
[4]Lamont-Doherty Earth Observatory, 61 Route 9W, P.O. Box 1000, Palisades NY 10964, USA.
[5]Present address: ExxonMobil Upstream Research Company, New Play Concepts, 3120 Buffalo Speedway, P.O. Box 2189, Houston TX 77252-2189, USA.
[6]Department of Earth Science, Rice University, Keith-Wiess Geological Labs, 6100 Main Street, Houston TX 77005, USA.
[7]Department of Geology and Geophysics, University of Wyoming, 1000 E. University Way, Laramie WY 82071-3006, USA.
[8]Department of Geology, University of Leicester, University Road, Leicester LE1 7RH, United Kingdom.

Initial receipt: 20 January 2006
Acceptance: 13 April 2007
Web publication: 24 July 2007
Ms 210SR-110

INTRODUCTION

The Newfoundland margin constitutes the western half of the well-studied Newfoundland–Iberia nonvolcanic margin pair. This conjugate margin system is a type example of nonvolcanic rifting wherein continental breakup is associated with little if any synrift magmatism. Previous Ocean Drilling Program (ODP) legs on the Iberia margin (e.g., Legs 103, 149, and 173), together with coincident geophysical data, have revealed that the final stages of rifting were in part accommodated by the exposure of subcontinental mantle at the seafloor between thinned continental crust and oceanic crust (Boillot et al., 1987; Chian et al., 1999; Krawczyk et al., 1996; Sawyer, Whitmarsh, Klaus, et al., 1994; Whitmarsh, Beslier, Wallace, et al., 1998).

To understand the entire rift system, a characterization of the conjugate Newfoundland margin is also necessary (Fig. **F1**). Several key questions about this margin have remained unresolved. One of the most important is the origin of an enigmatic section of basement (hereafter called transitional basement) that lies between unambiguous continental crust and the earliest presumed oceanic crust in the region of magnetic anomalies ~M3 and M0 on the Newfoundland margin (Keen et al., 1987; Srivastava et al., 2000; Tucholke et al., 1989). Three interpretations for transitional basement have been proposed:

1. Slow-spreading oceanic crust (Keen and de Voogd, 1988; Srivastava et al., 2000; Sullivan and Keen, 1978);
2. Thinned, possibly intruded continental crust (Enachescu, 1992; Lau et al., 2006b; Tucholke et al., 1989; Van Avendonk et al., 2006); and
3. Exhumed subcontinental mantle, similar to what is observed off Iberia (Tucholke et al., in press).

In seismic reflection sections, this crustal domain appears seismically transparent and is overlain by a set of bright reflections that include the U reflection, a seismic horizon observed throughout the Newfoundland Basin over both continental and transitional basement (Fig. **F2**). This horizon has been used to constrain the rifting history (Tucholke et al., 1989, in press). Learning the nature and age of these bright reflections is important for attaining a better understanding of both margins.

In addition to recording some of the tectonic history of the Newfoundland margin, the stratigraphic record encountered at ODP Site 1276 also contains information on the paleoceanography of this region. For example, another target of drilling at Site 1276 was Horizon A^U, which has been interpreted to be associated with the onset of strong abyssal circulation in the North Atlantic Ocean (Miller and Tucholke, 1983; Tucholke and Mountain, 1979). This paleoceanographic event is thought to represent erosion along the margins of the North Atlantic, followed by deposition of large sedimentary drifts (Jansa et al., 1979; Tucholke and Mountain, 1979; Wold, 1994). The A^U reflection is observed throughout the Newfoundland Basin, so learning its age and nature is important for understanding regional paleoceanography. Further analysis of core data and work on the seismic stratigraphy of this part of the Newfoundland Basin since ODP Leg 210 has revealed that there are two possible candidates for the A^U reflection in the vicinity of Site 1276 (**Tucholke and Sibuet,** this volume) (Fig. **F2,** A^{U1} and A^{U2} reflections). By establishing a link between core and seismic data at Site 1276 for

F1. Bathymetric maps of the Newfoundland margin, p. 20.

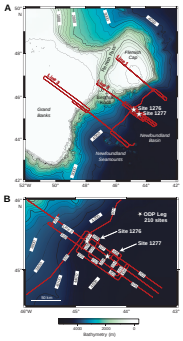

F2. Prestack time migration of SCREECH Line 2, p. 21.

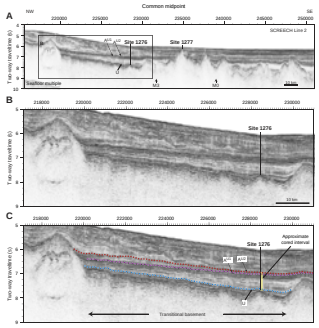

this interval, we can place some constraints on this aspect of the postrift history.

To investigate these features prior to drilling, new geophysical data were collected during July and August, 2000, on the Newfoundland margin in positions conjugate to Iberia drilling and geophysical transects, based on the reconstructions of Srivastava et al. (2000) (Funck et al., 2003; Hopper et al., 2004; Lau et al., 2006a, 2006b; Shillington et al., 2006; Van Avendonk et al., 2006) (Fig. F1). Velocity models created from wide-angle seismic data acquired during the Studies of Continental Rifting and Extension on the Eastern Canadian Shelf (SCREECH) experiment suggest that transitional basement is likely thinned, possibly intruded continental crust in its landward part and exhumed mantle in its seaward part (Lau et al., 2006b; Van Avendonk et al., 2006). SCREECH geophysical data were used to select and justify drilling targets on the Newfoundland margin. Drilling on the Iberian margin during ODP Legs 103, 149, and 173 had delineated the nature of basement within the zones of thinned continental crust and exhumed subcontinental mantle by sampling basement highs. To complement this information, the proponents of Leg 210 drilling proposed a deep hole away from basement highs on the Newfoundland margin. The hole was intended both to recover an extensive sedimentary record over transitional basement (from the upper Oligocene through the oldest sediments) and to sample the transitional basement. The deep sedimentary record should provide data that can be used to constrain the timing and character of events associated with late stages of rifting and early seafloor spreading.

Drilling at Site 1276 recovered 936.9 m of core dating from the early Oligocene to the earliest Albian–latest Aptian between 800.0 and 1736.9 meters below seafloor (mbsf), but it did not reach basement (Shipboard Scientific Party, 2004). Two diabase sills were encountered in the lowermost recovered sedimentary section at 1612.7–1623.0 mbsf and at 1719.2 to >1736.9 mbsf; minor, thin (3–31 cm thick) sills occur 7–14 m above the lower sill. The sills are separated by 100 m of sediment that included an ~17-m-thick section of sediments with very low velocities (~1.7 km/s) and densities (~2.05 g/cm^3). This layer has been interpreted as undercompacted, and its properties might be related to the emplacement of the postrift sills (Karner and Shillington, 2005; Shipboard Scientific Party, 2004). The upper sill is ~10 m thick, and drilling terminated ~18 m into the lower sill, so its full thickness is unknown. Postcruise work has demonstrated that the sills are postrift (Albian, ~105–98 Ma) (Hart and Blusztajn, 2006; Karner and Shillington, 2005). From preliminary analyses during and immediately following Leg 210, the interval containing sills and undercompacted sediments was estimated to lie at the approximate depth of the U reflection and other bright reflections overlying transitional basement, although synthetic seismograms did not establish a definitive link between either the sills or undercompacted sediments and the U reflection (Shipboard Scientific Party, 2004).

The thick section of cored sediments and the recovery of two postrift sills at Site 1276 present an excellent opportunity to better constrain the history of the Newfoundland–Iberia conjugate margins. A necessary first step to extrapolating detailed information on age and lithology at Site 1276 to the remainder of the Newfoundland Basin is to make a link between core data and coincident seismic reflection data. Logging data are traditionally used to link these data sets by measuring in situ geophysical properties of borehole lithologies at a scale intermediate between seismic and core data. However, logging data could not be

collected at Site 1276 because of unstable hole conditions. In lieu of logging data, we present results that link Site 1276 to coincident seismic reflection data by the creation of synthetic seismograms from core physical property measurements. We use the reflectivity method, which includes the contribution of interbed multiples and frequency-dependent interaction in the presence of thin layering (see Kennett, 1983, for a full description). These effects are potentially important given the presence of thin layers associated with large velocity variations at Site 1276. Excellent core recovery (average = 85%) throughout Site 1276 afforded measurement of a detailed physical property data set to use for this purpose. Such data have been successfully applied to the creation of synthetic seismograms for other ODP sites (Bloomer and Mayer, 1997; Edwards, 1998; Norris et al., 2001; Zühlsdorff and Spiess, 2001). Our method includes the following steps:

1. Processing of laboratory physical property measurements to explore biases in sampling,
2. Establishment of an initial time-depth tie for the top of the cored section (which begins at 800 mbsf) by velocity modeling of multichannel seismic (MCS) reflection data,
3. Creation of synthetic seismograms below 800 mbsf using edited laboratory measurements of velocity and density, and
4. Comparison of the synthetic and real seismic reflection data to link major reflections to specific features in the cored section and to refine the linkage between the top of cored section and two-way traveltime (TWT).

DATA ACQUISITION AND PROCESSING

Seismic Data

The SCREECH survey acquired >3000 km of MCS, magnetic, gravity, and multibeam bathymetric data and 1000 km of wide-angle seismic reflection/refraction data off Newfoundland (Fig. **F1**). This was a two-ship program with MCS, magnetic, gravity and bathymetric data acquired aboard the *Maurice Ewing* (Cruise 00-07) and wide-angle seismic reflection/refraction data acquired by ocean-bottom seismometers/hydrophones deployed and retrieved from the *Oceanus* (Cruise 359-2). Coincident MCS reflection data and wide-angle seismic reflection/refraction data were collected along three primary transects (Fig. **F1**). MCS data were also collected on lines parallel and perpendicular to all transects, including the locations of both Leg 210 sites indicated by white stars in Figure **F1.** MCS data were recorded on the 6-km, 480-channel streamer of the *Maurice Ewing;* these data have a sampling interval of 4 ms, a shot-spacing of 50–62.5 m, a fold of 45–60, a recording length of ~16 s, and a common midpoint (CMP) spacing of 6.25 m. The tuned, 8540-in^3, 20-gun array of the *Maurice Ewing* was the seismic source for both wide-angle and MCS seismic data. SCREECH Line 2, the central of the three primary transects, crosses Leg 210 Sites 1276 and 1277 (Figs. **F1, F2**), and the MCS data from this line are used for comparison with synthetic seismograms created from laboratory measurements. The profiles presented here were created by prestack time migration; a full description of processing is given by Shillington et al. (2004).

Core Data

Lithology

At Site 1276, 936.9 m of core were recovered between 800.0 and 1736.9 mbsf (Shipboard Scientific Party, 2004). Cored sediments range in age from early Oligocene to earliest Albian–latest Aptian. The sedimentary section was subdivided into five units based on variations in lithology and breaks in age as defined by biostratigraphy (Fig. F3). A brief description of each unit is given below; a complete description of the lithology and biostratigraphy can be found in Shipboard Scientific Party (2004).

1. Lithologic Unit 1 (753–864.7 mbsf [includes wash Core 210-1276A-1W from 753 to 800 mbsf], middle Eocene–lower Oligocene): Unit 1 is hemipelagic, burrowed mudstone and claystone (~85%) with minor amounts of disorganized muddy sandstone and sandy mudstone deposits (~8%) and grainstone beds (~7%) emplaced by turbidity currents and debris flows. Soft-sediment deformation features are common.
2. Lithologic Unit 2 (864.7–929.3 mbsf, upper Paleocene–middle Eocene): This unit is dominated by beds that range from grainstone and calcareous sandstone (~40%) to marlstone (~40%), interlayered with lesser amounts of mudrock (~20%). Grainstone and sandstone contain significant amounts of $CaCO_3$ (typically between 30 and 60 wt%), and there is a high proportion of graded beds deposited from turbidity currents.
3. Lithologic Unit 3 (929.3–1028.0 mbsf, lowermost Campanian–upper Paleocene): Unit 3 consists primarily of mudstone and claystone (~80%) deposited by gravity flows in dominantly graded beds. It also contains subordinate grainstone and calcareous sandstone, marlstone, calcareous siltstone, and sandy mudstone. Grainstone is much less abundant than in Unit 2.
4. Lithologic Unit 4 (1028.0–1067.2 mbsf, Turonian–upper Santonian): Unit 4 is mostly siliciclastic muddy sandstone, sandstone, mudstone, sandy mudstone, and siltstone. These rocks have reddish hues and are highly bioturbated.
5. Lithologic Unit 5 (1067.2–1736.9 mbsf, uppermost Aptian/lowermost Albian–Turonian): Overall, Unit 5 is dominated by mudrock (60%–90%) deposited by gravity flows. This thick unit is divided into three subunits. Subunit 5A (1067.2–1129.8 mbsf) is characterized by gravity-flow deposits interspersed with minor amounts of hemipelagic sediments. Subunit 5B (1129.8–1502.1 mbsf) is dominantly hemipelagic, variably calcareous, and carbon-rich mudrock with minor turbidites. Subunit 5C (1502.1 mbsf to the total depth of the hole) contains poorly organized gravity-flow deposits that include sandy debris and graded beds. Diabase sills occur at 1612.7–1623.0 mbsf (Subunit 5C1) and 1719.2 to >1736.9 mbsf (Subunit 5C2) within these sediments. The upper sill is ~10 m thick. The thickness of the lower sill is unknown because drilling terminated before reaching its base, but it is at least 18 m thick. Whole-rock Ar^{40}/Ar^{39} radiometric dating yielded ages of 105.95 ± 1.78 and 104.7 ± 1.7 Ma (average = 105.3 Ma) for samples from the upper sill and 99.7 ± 1.8 Ma and 95.9 ± 2.0 Ma (average = 97.8 Ma) for samples from the lower sill (Hart and Blusztajn, 2006).

F3. Vertical and horizontal *P*-wave velocity and density, p. 22.

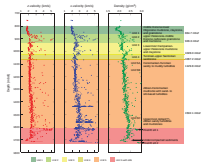

Approximately 96 m of sediment lie between the two sills, including a ~17-m-thick interval from 1693 to 1710 mbsf that has very low velocities (~1.7 km/s) and densities (2.05 g/cm^3). The explanation for the undercompaction of these sediments is still uncertain, but it is possible that the sills sealed off this interval and thus prevented normal compaction (Karner and Shillington, 2005; Shipboard Scientific Party, 2004).

Physical Property Measurements

As part of the standard shipboard analysis of all recovered cores, laboratory measurements of physical properties (e.g., density, compressional [*P*]-wave velocity, thermal conductivity, natural gamma radiation, etc.) were made on whole cores and/or selected samples. Of particular value to the present study are velocity and density (Fig. F3). Horizontal (*x*) and vertical (*z*) velocities were measured on representative sediment and rock samples every ~2 m throughout the recovered section (Shipboard Scientific Party, 2004). Cubes of rock ~8 cm^3 in size were cut from the working half of the core, and *P*-wave velocity was measured in three directions using the *P*-wave velocity sensor 3 modified Hamilton Frame velocimeter. An acoustic signal of 500 kHz is transmitted and received between two transducers, passing though the sample, whose thickness is measured by a digital caliper. We chose to use the measurements of vertical velocity to create synthetic seismograms because they most closely approximate the path of seismic waves recorded in the seismic reflection data. This choice has implications for the time-depth relationship established below 800 m. The difference between vertical and horizontal velocity increased downhole from ~4%–5% at 800 mbsf to ~10% in the deepest sediments (Shipboard Scientific Party, 2004). Horizontal velocities are often faster in sediments because of grain orientation and cementation along near-horizontal bedding planes. The longest offset arrivals in the MCS reflection data will have a significant contribution from horizontal velocities. Therefore, the use of vertical velocities indicates that the depth-time relationship established below 800 mbsf from laboratory measurements will represent the slow end-member.

Two types of density measurements were taken on each core: (1) gamma ray attenuation (GRA) bulk density and (2) moisture and density (MAD). GRA data are evenly spaced measurements of density obtained over the full core before splitting. Although this procedure provides continuous, finely spaced measurements (~2.5 cm), the consolidated sediments and rocks retrieved using rotary core barrel drilling typically fracture when they are recovered, leading to breaks in the core, reduced core volume, and significant artificial variations in the density data. GRA density measurements are also too low because recovered cores do not completely fill the core liner (Shipboard Scientific Party, 2004). These artificial variations in density would cause significant noise when computing synthetic seismograms, and thus the GRA densities were not used. The MAD technique determined wet and dry bulk density, grain density, and porosity on discrete samples taken from every section of each core. Because the samples analyzed were small and hand-selected, they were not as compromised by the fractures that degrade the GRA density measurements, although they are affected by decompaction. Also, because of noncontinuous sampling and imperfect (85%) core recovery, they do not sample the details of density and velocity changes that would be measured by downhole logging. Densities were obtained from the same samples measured for velocity, so any

sampling biases will be present in both data sets. Nonetheless, because these data contain fewer artificial variations because of core breaks or core diameter compared to GRA data, they are more suitable for our purposes.

Processing of Physical Property Data

The use of physical property data instead of traditional sonic and density logs requires several additional considerations to ensure that velocity and density measurements are used in a way that best represents the overall core properties:

1. First, velocities measured on samples that were described as concretions by sedimentologists were removed. This included eight measurements in the hole with vertical component velocities ranging from 2.126 to 4.625 km/s. Concretions are small and anomalous, and thus they are unlikely to contribute to the bulk seismic properties of the subsurface at the frequencies of MCS data considered here (i.e., ~10–100 Hz). If these data were included in the velocity and density functions used to create synthetic seismograms, they could significantly affect the seismograms, which are sensitive to small velocity perturbations. Because these measurements comprise only 8 of 533 data points, their exclusion does not impact the overall depth-time relationship established below 800 mbsf using the remaining data.
2. Another important consideration when using laboratory velocities is the difference in velocity expected at in situ pressures versus atmospheric pressures where the velocities are measured. When cores are brought to the surface, they undergo decompaction and fracturing because of the change in confining pressure and drilling disturbance; these effects lower the bulk modulus of cored sections, which leads to a decrease in *P*-wave velocity (Carlson et al., 1986). As with our use of vertical velocities, the decompaction effects will shift our velocity model toward the slow end-member. This effect is considered when we link synthetic seismograms to reflection profiles.
3. Finally, the physical property measurements were made on hand-selected samples spaced at ~2 m, and thus they might contain biases toward anomalously high- or low-velocity material (Carlson et al., 1986) (for comparison, the sampling interval of the downhole wireline Sonic Digital Tool used for acquiring in situ measurements during logging is 6 inches [0.1524 m]). The danger of bias in laboratory measurements certainly arises in turbidites, where a variety of lithologies occur over a small range in depth. We examined this issue by measuring horizontal velocity through turbidites at 2-cm intervals on the uncut archive half of several cores (Shipboard Scientific Party, 2004). Only horizontal velocities were measured because the measurement of vertical velocities would have required cutting the cores at 2-cm intervals. These measurements show that velocities change downward through the turbidite sequences, from lower velocities (~2.0–2.5 km/s) in finer grained mudrocks at the top of the turbidites to higher velocities in the fine-grained sandstones (~4.5–5.0 km/s). Velocities decrease within the coarse-grained bases of the turbidites (~3.0–4.5 km/s).

These results show that care must be taken when interpolating physical property measurements between locations. For example, a measurement on a sample from a thin interval of a particular lithology could be extrapolated to exist over 2 m, or more in the case of gaps between cores. This could affect the reflection characteristics of a synthetic seismogram significantly, particularly if the measured velocity is much higher or lower than the average velocity trend. It may at least partially account for discrepancies between MCS data and synthetic seismograms created at sea during Leg 210. Those synthetic seismograms contained several bright reflections that could not be easily related to reflections in the MCS data (Shipboard Scientific Party, 2004). This was particularly true of synthetic reflections arising from within Unit 5, which is largely mudrock and corresponds to an interval of low-amplitude, discontinuous reflections in the MCS data (Shillington et al., 2004; Shipboard Scientific Party, 2004).

We tried three different approaches to processing physical property data in order to explore the effects of sampling bias on synthetic seismograms (Fig. **F4**):

1. All measured velocities and densities were included except for those from concretions. No modifications were made to the apparent vertical extent of each velocity or density measurement.
2. High-velocity (>3 km/s) measurements from thin (<1 m thick) intervals shallower than the upper sill were removed from Unit 5 (1067.2–1612.7 mbsf), where high-velocity materials were comparatively unrepresentative.
3. The thicknesses associated with physical property measurements on samples taken from high-velocity (>3 km/s) beds throughout the cored section were adjusted to match the thicknesses of beds with corresponding lithologies from which they were sampled (Shipboard Scientific Party, 2004).

The processing steps described above screen the data points in different ways to account for the presence of potentially anomalous samples and to test the effects of sample bias.

The final step was to create an "earth model" consisting of a series of layers, and it was ultimately used for the calculation of synthetic seismograms. These layers were interpreted by hand within the Nucleus software package to group together similar velocities and densities; 252 layers were included in this analysis. Given that there are 533 input data points, there is an average of <2 data points per layer. For each layer, *P*- and *S*-wave velocity, density, and *P*- and *S*-wave attenuation (Q_P and Q_S, respectively) must be given. The density and *P*-wave velocity assigned represent average values calculated between the interpreted top and base of the layer based on input data points. The result of this averaging step is that layers in the final earth model are assigned velocities that are neither as high nor as low as velocities in the original velocity function (Fig. **F5**). Both the input data points and the average velocities assigned to the layers in the earth model are shown in Figure **F6**. *S*-wave velocity is estimated from *P*-wave velocity. We use a Q_P of 1000 and a Q_S of 5000 for water, 200 and 100 for sediments, and 400 and 100 for sills (Fuchs and Muller, 1971; Minshull and Singh, 1993).

We generated synthetic seismograms for earth models derived from each of the three scenarios described above (Fig. **F6**) to examine the robustness of the reflections generated and to test their sensitivity to

F4. Three scenarios for processing physical property measurements, p. 23.

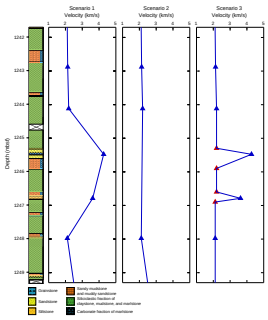

F5. Creation of earth model, p. 24.

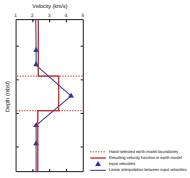

F6. Velocity functions used to calculate reflection coefficient series, p. 25.

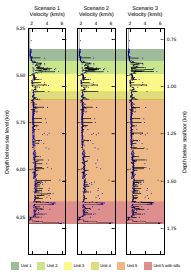

potential sampling biases in laboratory measurements. All three cases are discussed in "Results and Discussion," p. 10.

SYNTHETIC SEISMOGRAMS

The reflectivity method that is used to calculate synthetic seismograms (Kennett, 1983) includes most aspects of the wavefield expected for a given one-dimensional (1-D) velocity structure, including interbed multiples and frequency-dependent interaction in the presence of thin layering. These effects are not accounted for when generating synthetics by simple zero-offset convolution. Given the presence of thin beds at Site 1276, these effects are potentially important. Reflectivities and transmissivities are calculated in the *tau-p* domain for a series of layers with different velocities, densities, and attenuations using Kennett's algorithm as implemented by the commercial software package Nucleus (see Kennett, 1983, for a full description). The *tau-p* synthetic is transformed to the *x-t* domain using an inverse Radon transformation, yielding an *x-t* synthetic seismogram that consists of a prestack CMP gather. For comparison with the coincident MCS data, the synthetic CMP gather is corrected for normal moveout and stacked. The input for this method is the earth model described above and an estimate of the source wavelet, which is described below.

Source Wavelet Estimation

Two separate approaches were used to estimate the source wavelet: (1) deconvolution of the first seafloor multiple with the seafloor reflection and (2) source modeling of the gun array used during the acquisition of the reflection data. The first approach follows the method employed by Korenaga et al. (1997). The first seafloor multiple is deconvolved with the primary seafloor reflection after applying a spherical divergence correction for geometrical spreading. The second approach models the source signature (near- and far-field) using the size and arrangement of the air gun source. These methods produce estimates of the source wavelet that are similar to one another and to reflections from the seafloor, which is typically a simple, sharp interface and whose seismic response should approximate the source wavelet (Fig. F7). This consistency gives us confidence that our estimate of the source wavelet is accurate. We used the source wavelet estimated from the second method because the software used for that method is the same as used for the remainder of our calculations.

F7. Estimates of seismic source wavelet, p. 26.

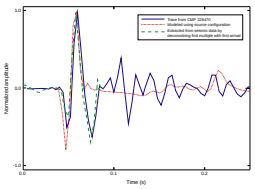

Estimating Reflection-Time Depth of the Top of Cored Section

A direct link between TWT and depth is typically obtained during logging operations by firing an air gun at the surface and recording the one-way traveltime to a geophone positioned within the borehole (i.e., a checkshot survey). Because the upper 800 m at Site 1276 were not cored or logged, this critical piece of information is missing from our analysis, and a tie between depth and the traveltime of some reflection must be established by other means. As described in the Leg 210 *Initial Reports* volume, the reflection with a positive peak at 6.982 s originally appeared to be the best candidate to make this link (Shipboard Scientific Party, 2004). Discontinuous, low-amplitude reflections lie above

this horizon and continuous, high-amplitude reflections are found below (Fig. F2). The depth to this horizon estimated from velocities obtained from semblance plots of MCS reflection data prior to drilling (~900 mbsf) was within 4% of the depth (864.7 mbsf) below which the lithology changed from mostly hemipelagic claystone (lithologic Unit 1) to consistently alternating layers of carbonate-cemented grainstone and mudstone (lithologic Unit 2). Some of the carbonate-cemented sandstones and claystones in Unit 2 have high velocities (up to 5.8 km/s) compared to the overlying hemipelagic claystones (~2–2.5 km/s) and thus were expected to produce high-amplitude reflections (Fig. F3). Because of these features, we chose this lithologic change to tie TWT to depth in the shipboard analysis (Shipboard Scientific Party, 2004). Below this horizon, the time-depth relationship was determined from laboratory measurements of *P*-wave velocity.

We have subsequently tested this tie between TWT and depth by creating a new velocity model from the MCS reflection data (red line, Fig. F8). Picks of horizons from eight adjacent CMP gathers near Site 1276 served as input into forward modeling using RAYINVR (Zelt and Smith, 1992). Nine horizons were interpreted and assigned picking errors of 8 ms; these included the prominent A^{U1} and U reflections. Iterative forward modeling and inversion of the 3796 data points provided a 1-D model with a chi-squared of 0.404 and a root-mean-square traveltime residual of 5 ms. The upper 500 m is characterized by low velocities (1.5–1.84 km/s) and a low-velocity gradient, and from 500 to ~820 mbsf the velocity increases to ~2.2 km/s with a slightly steeper gradient. This section is underlain by a rapid increase in velocity, reaching a maximum velocity of 2.55 km/s at 901 mbsf or 5.46 km below sea level. These high velocities correspond to the bright horizontal reflections at ~7 s TWT (Fig. F8). Beneath this section, velocities decrease again to 2.40 km/s, and then increase gradually to 2.65 km/s through the comparatively transparent section of sediments between 7.15 and 7.5 s. Below this section lies the bright U reflection. The section beneath U is marked by a rapid increase in velocities (modeled as 2.85–4.25 km/s from the MCS data).

To create synthetic seismograms, we used the velocities determined by the above analysis for the section above the shallowest core sample. Below the shallowest sample, we used laboratory measurements of velocity. From this model, we estimate that the shallowest in-place sample (800 mbsf, Core 210-1276A-2R) has an associated TWT of 6.954 s. (We exclude the wash Core 210-1276A-1W, which includes materials from unknown depths between 753 and 800 mbsf). In the following sections, we compare the waveforms of synthetic seismic reflection data to those of coincident seismic reflection data in order to further refine this depth-time tie.

F8. Velocity modeling of MCS reflection data, p. 27.

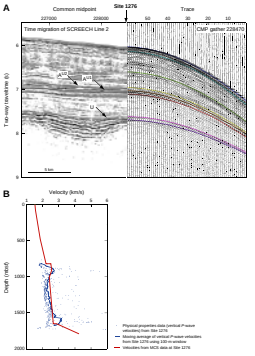

RESULTS AND DISCUSSION

Differences between Synthetics from Scenarios 1, 2, and 3

The method described above yields a set of three synthetic CMP gathers that can be compared with data near Site 1276 (Fig. F9). All three sets of synthetic data reproduce most of the first-order features seen in observed data, including the series of bright horizontal reflections observed around ~7 s and the U reflection and underlying bright

F9. Synthetic seismograms for Scenarios 1, 2, and 3, p. 28.

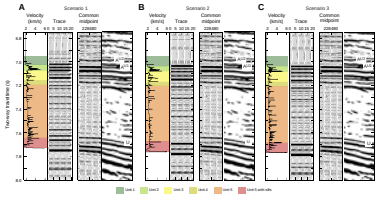

reflections toward the base of the stratigraphic section (~7.62–7.75 s). The reflections corresponding to Units 1–4 are similar between the three scenarios, despite the modifications made to the layer thicknesses associated with high velocities in Scenario 3. However, there are differences among the three scenarios for Unit 5. In the synthetic for Scenario 1 (Fig. F9A), a series of bright reflections can be observed in Unit 5 that do not appear to correspond to reflections in the MCS reflection data (e.g., ~7.3, 7.35, 7.39, 7.57, and 7.62 s). These reflections are caused by high-velocity measurements, some of which are from very thin lithologic intervals. In Scenario 2, many of these reflections are no longer present because all high-velocity (>3 km/s) measurements from thin (<1 m) intervals in this unit were removed (Fig. F9B). The complete elimination of some measurements from Unit 5 makes this synthetic the least realistic, but it provides a useful way to consider the effects of high-velocity measurements. Scenario 3 represents a compromise between these two end members, where the thickness associated with high-velocity measurements has been adjusted to better approximate the thickness of corresponding lithologies in the core. In this synthetic, reflections are found at TWTs similar to those in Scenario 1, but they are typically lower in amplitude (Fig. F9C). Although all three sets of synthetics reproduce the first order features, Scenario 3 appears to best represent subtle waveform characteristics observed in coincident reflection data in Unit 5 above the sills (Fig. F9C). Thus, we use this synthetic for the detailed discussion of links between seismic and core data that follows.

Core-Seismic Correlation

Below, we consider three alternative correlations between synthetic-seismogram Scenario 3 and reflection data, as illustrated in Figure F10. These correlations are identical at the base of the hole but differ in the precise linkages made between synthetic and observed reflections for Units 1–4. The largest uncertainty in correlations occurs in this portion of the hole because of the absence of a definitive depth-time link for the top of the hole, as discussed earlier. After considering the Unit 1–4 correlations, we discuss correlations between the synthetic seismogram and reflection data for Unit 5, with particular focus on the U reflection and the two postrift sills at the base of Site 1276.

F10. Three interpretations for Scenario 3 synthetic seismogram, p. 29.

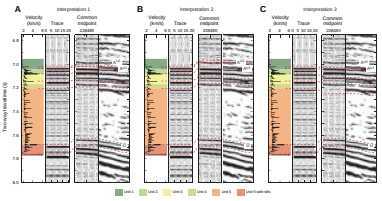

Lithologic Units 1–4

Lithologic Unit 1 is dominantly represented by mudrock, and the associated velocity and density measurements are correspondingly homogeneous (Fig. F3). As a result, primarily low-amplitude reflections appear in the synthetic seismogram for this interval (Fig. F9). However, one bright reflection (7.02 s in Fig. F10) is generated in synthetic seismograms near the base of lithologic Unit 1; this results from carbonate-cemented claystones and sandstones that are associated with velocities as high as 3.659 km/s between 841.3 and 852.5 mbsf. In contrast to Unit 1, laboratory measurements of density and velocity taken from Units 2–4, particularly Unit 2, show dramatic changes in velocity (1.961–5.545 km/s) and density (1.95–2.647 g/cm^3) (Fig. F3) that produce a series of high-amplitude reflections in the synthetic seismogram (7.04–7.23 s) (Fig. F9). These variations in physical properties and the resulting bright reflections in the synthetic seismogram are generated by the interlayering of high-velocity carbonate-cemented claystones

and sandstones that are found in turbidites (20–140 cm thick) with low-velocity marlstone and claystone. Strong velocity contrasts are also found, to a lesser extent, in Units 3 and 4. The deepest reflection in this bright series is located at ~7.23 s in the synthetic seismogram and appears to arise from a negative impedance contrast at the base of Unit 4.

Because of the nature of the velocity and density measurements used to generate the synthetic seismograms and the lack of a definitive depth-time tie (normally supplied by a checkshot survey), we can envisage three different possible correlations between the reflections in the synthetic seismogram produced by Units 1–4 and the coincident seismic reflection data:

1. Interpretation 1: The Unit 1/2 boundary correlates with Reflection A^{U1} (~7.02 s), and the Unit 4/5 boundary correlates to the apparent seismic unconformity at ~7.19 s in reflection data; this correlation of the Unit 4/5 boundary was originally proposed in the Leg 210 *Initial Reports* volume (Shipboard Scientific Party, 2004) (Fig. **F10A**).
2. Interpretation 2: The Unit 1/2 boundary corresponds to Reflection A^{U2} (~6.98 s), and the Unit 4/5 boundary corresponds to the reflection at ~7.16 s (Fig. **F10B**). This correlation of the Unit 1/2 boundary was originally proposed in the Leg 210 *Initial Reports* volume (Shipboard Scientific Party, 2004).
3. Interpretation 3: The Unit 1/2 boundary corresponds to the reflection beneath Reflection A^{U1} (~7.04 s), and the Unit 4/5 boundary corresponds to the reflection at ~7.22 s (Fig. **F10C**).

To determine which of these three interpretations is most likely, we compare reflection characteristics between the synthetic seismogram and MCS data and consider the implications for velocity structure implied by each interpretation. For Interpretation 1, the match between reflection characteristics in the synthetic seismogram and MCS data (Fig. **F10A**) is good overall. Reflection A^{U1} is lower in amplitude in the MCS data than in the synthetic seismogram. The brightest reflections in the synthetic seismogram, which are associated with Unit 2, correlate with the brightest reflections in the seismic reflection data. Below this, a series of reflections with slightly lower amplitudes are observed in both the synthetic seismogram and the MCS data, and the Unit 4/5 boundary is matched to the deepest reflection in the bright package between 7.04 and 7.19 in the reflection data.

Matches between reflections in the synthetic seismogram and MCS reflection data for Interpretation 2 are generally poor for Units 1, 2, and the upper portion of Unit 3 but are very good for Units 3 and 4 (Fig. **F10B**). Although the amplitudes of the Unit 1/2 boundary reflection in the synthetic seismogram and Reflection A^{U2} in the MCS data are more similar than the correlation in Interpretation 1 (Fig. **F10A**), the underlying reflections associated with Unit 2 in the synthetic seismogram are much stronger than the corresponding reflections in the seismic data.

Finally, correlations between reflections in the synthetic seismogram and reflection data for Interpretation 3 are relatively good for Units 1, 2, and 3 but are poor for Unit 4 (Fig. **F10C**). The strong reflections arising in the synthetic seismogram from the Unit 1/2 boundary and from Unit 2 correspond to strong reflections in the seismic reflection data. However, the reflections associated with the base of Unit 4 in the synthetic seismogram have higher amplitudes than the corresponding reflections in the MCS data.

Each of these interpretations also carries implications for the velocity structure between the seafloor and the lithologic Unit 1/2 boundary (~865 mbsf) and between this boundary and the underlying upper sill (the U reflection at 1613 mbsf, see "Lithologic Unit 5, Including Sills and Undercompacted Sediments," p. 14). We can compare the velocity structure implied by each of these interpretations with the velocities estimated by modeling MCS reflection data described above in "Estimating Reflection-Time Depth of the Top of Cored Section," p. 9 (Fig. F8). We chose to compare average velocities above and below 865 mbsf, the Unit 1/2 boundary (Fig. F10). Modeling of MCS reflection data yields an average velocity of 1839 m/s between the seafloor (6.04 s) and 865 mbsf and of 2508 m/s between this level and the U reflection. The following velocities are implied for each of these two intervals by each of the interpretations presented in Figure F10: Interpretation 1: 1765 m/s and 2473 m/s; Interpretation 2: 1840 m/s and 2319 m/s; Interpretation 3: 1648 m/s and 2579 m/s (Table T1; Fig. F11). If the other synthetic seismograms in Figure F9 (Scenarios 1 and 2) were used for these interpretations, the implied velocities would only vary by ≤15 m/s. Interpretation 1 predicts velocities above and below 865 mbsf that are close to those estimated by modeling MCS reflection data, with differences of ~74 m/s above and ~35 m/s below this level. Interpretation 2 predicts average velocities above 865 mbsf that are very close to those from MCS reflection modeling (within ~1 m/s) but much lower (~189 m/s) below. Finally, Interpretation 3 predicts much lower velocities (~191 m/s) above 865 mbsf than those estimated by modeling of MCS reflection data but velocities that are somewhat higher (~71 m/s) than modeled velocities below this level (Table T1; Fig. F11).

Based on both reflection characteristics and implied velocity structure, we favor Interpretation 1. This correlation provides an acceptable fit between reflection characteristics for lithologic Units 1–4 and implies a realistic velocity structure throughout the sedimentary section. Conversely, for Interpretation 2, the mismatch between reflection characteristics for Unit 2 and the unrealistically low velocities implied below 865 mbsf suggest that this interpretation is not viable. Finally, the mismatch between reflections at the base of Unit 4 and the low velocities implied for the interval above 865 mbsf argue against Interpretation 3. The results of adjusting the synthetic seismogram up to match the observed data, consistent with Interpretation 1, are shown in Figure F12.

Tucholke and Sibuet (this volume) have identified two possible reflections (A^{U1} and A^{U2}) that might correspond to Horizon A^U observed farther south in the main North Atlantic basin (Fig. F2). The A^U reflection there correlates with a hiatus near Eocene/Oligocene boundary and is commonly expressed as a seismic unconformity (Miller and Tucholke, 1983; Tucholke and Mountain, 1979). Thus the reflection has been correlated to the onset of strong abyssal circulation in the North Atlantic Ocean (Miller and Tucholke, 1983). The association of the A^{U1} reflection with the Unit 1/2 boundary described above for Interpretation 1 implies that this reflection does not correspond to Horizon A^U. Wood et al. (submitted [N1]) conducted a detailed study of the nannofossil biostratigraphy of the interval around the Unit 1/2 boundary and found that it corresponded to a hiatus of between 1.2 and 6.9 m.y. in the middle Eocene (47.3–40.4 Ma). This timing is some ~6 m.y. older than predicted for the onset of circulation in the North Atlantic Ocean. Furthermore, seismic sequence characteristics associated with the flow of abyssal currents, particularly sediment waves, are developed above the A^{U2} reflection. Thus Tucholke and Sibuet (this volume) suggest

T1. TWT and average velocities, p. 32.

F11. Comparison of velocities above and below Unit 1/2 boundary, p. 30.

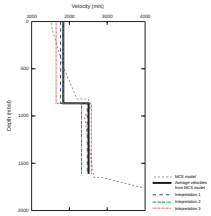

F12. Seismic horizons on a section of SCREECH Line 2, p. 31.

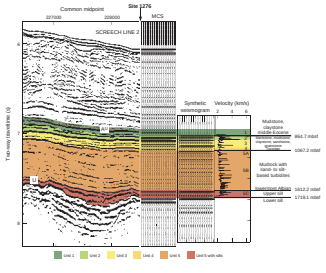

that the A^{U2} reflection at ~6.96 s is more likely to correlate with Horizon A^{U} farther to the south in the western North Atlantic. In Interpretation 1, the A^{U2} reflection lies close to the top of the cored interval beginning at 800 mbsf, and according to shipboard biostratigraphy, this level dates to the latest Eocene–earliest Oligocene (Shipboard Scientific Party, 2004).

The correlation between the reflection arising from the Unit 4/5 boundary and the reflection at ~7.19 s in the seismic data agrees well with shipboard biostratigraphy. This reflection truncates underlying reflections over much of the transition zone and thus appears to represent an unconformity (Fig. **F2**). Biostratigraphic data suggest a period of either very slow sedimentation or a hiatus at about this level (Campanian–Turonian), although this is not well constrained because some cores at this boundary were barren of microfossils (Shipboard Scientific Party, 2004).

Lithologic Unit 5, Including Sills and Undercompacted Sediments

In contrast to the bright reflections predicted for lithologies in Units 2–4, much lower amplitude reflections are observed in the synthetic seismogram associated with Unit 5 (7.24–7.68 s, Fig. **F10**), which is dominated by mudrock. Velocity and density in this interval show much less variation than in the overlying lithologic units (Shipboard Scientific Party, 2004) (Fig. **F3**), and weak reflections found in this interval are caused by velocity and density variations associated with intermittent turbidites. According to our interpretation, this section of low reflectivity likely corresponds to the low-amplitude interval in the coincident seismic reflection data spanning 7.19–7.62 s (Fig. **F10A**).

The velocity and density structure at the base of Site 1276 is considerably more complicated than in the remainder of the hole, with variations of more than 4.0 km/s in velocity and 2 g/cm^3 in density over tens of meters in depth (Fig. **F3**). These changes in core properties are associated with the presence of both diabase sills (tops at 1612.7 and 1719.2 mbsf) and a thin, ~17-m-thick interval of undercompacted sediments (1693–1710 mbsf). The large changes in velocity and density associated with these features result in high-amplitude reflections in the synthetic seismogram. A strong reflection beginning at 7.68 s in the synthetic is caused by a combination of the positive and negative impedance contrasts from the top and base of the upper sill, respectively (Fig. **F10A**). At 7.76 s, an even stronger reflection is predicted in the synthetic seismogram, caused by a positive impedance contrast between the base of the undercompacted sediments and the top of the lower sill. Overall, the pattern of synthetic reflections closely resembles the U reflection and the underlying reflections in the MCS reflection data (Fig. **F10**), implying that the U reflection at Site 1276 is created by the upper 10-m-thick diabase sill.

Implications for Depth-Time Relationship Derived beneath 800 mbsf

For all of the synthetic-seismic correlations discussed above, the difference in TWT for reflections in the synthetic seismogram and the MCS data increases progressively with depth. For example, in Scenario 3, Interpretation 1, the difference increases from 21 ms at the level of

the A^{U1} reflection to 62 ms at the U reflection, yielding a total change of 41 ms (Fig. F10A). This indicates that the average velocity used to create the synthetic seismogram is too low, and this low velocity is likely is an artifact of the velocity function derived from laboratory measurements. As mentioned earlier, samples from cores brought to the surface from depth undergo decompaction and microfracturing, causing laboratory measurements of velocity and density taken at atmospheric pressure to have lower values than they would have in situ. Additionally, we used vertical velocities to create our synthetic seismograms. Sediments at Site 1276 exhibit increasing transverse anisotropy with depth, so that horizontal velocities were greater than vertical velocities (Shipboard Scientific Party, 2004). Thus, the large offsets recorded in this MCS reflection data set would have a contribution from comparatively high horizontal velocities. All of these effects suggest that laboratory measurements of vertical velocity provide a slow-velocity end-member for depth-time conversion. To resolve the difference in TWT for the interval noted above (assuming the correlation in Interpretation 1, Fig. F10A), an ~10%–11% increase in velocity would be required for synthetic seismogram Scenarios 2 and 3 (where high velocities were removed or the thickness associated with them were modified), and a 3% increase would be needed for Scenario 1. Such shifts are consistent with the effects described above.

CONCLUSIONS

We have linked core data at Leg 210 Site 1276 with coincident seismic reflection data from the SCREECH experiment by creating synthetic seismograms from shipboard laboratory measurements of velocity and density. Because laboratory measurements were made on discrete, hand-selected samples, in contrast to the regularly spaced measurements included within a logging data set, some additional processing was required. The resulting synthetic seismograms demonstrate the following ties:

1. The lithologic Unit 1/2 boundary corresponds to a bright reflection observed at ~7.02 s in seismic reflection data (Figs. F2, F10A; Reflection A^{U1}). Seismic stratigraphic character and biostratigraphy (Tucholke and Sibuet, this volume; Wood et al., submitted [N1]) indicate that the A^{U1} reflection does not correlate with the regional Horizon A^{U} reflection observed in the main North Atlantic basin to the south. Instead, a shallower reflection at 6.96 s (A^{U2}) most likely corresponds to Horizon A^{U} (Tucholke and Sibuet, this volume). This reflection lies at the top of the cored section at Site 1276 (~800 mbsf) and dates approximately to the Eocene/Oligocene boundary.
2. The bright reflections found between 7.02 and 7.19 s in seismic reflection data result from interlayering of carbonate-cemented sandstone and claystone with mudrock in Units 2–4.
3. The base of Unit 4 correlates with an apparent seismic unconformity at ~7.19 s in seismic reflection profiles across Site 1276. Shipboard biostratigraphy suggests either a hiatus or low sedimentation rates in this interval.
4. Finally, our synthetic seismograms demonstrate that the prominent U reflection at Site 1276 is caused by the shallower of two postrift igneous sills. An underlying strong reflection is caused

by a second, deeper postrift sill. Further work will be required to understand potential relationships between igneous sills and the U reflection across the Newfoundland Basin away from Site 1276.

ACKNOWLEDGMENTS

This research used samples and data provided by the Ocean Drilling Program (ODP). ODP is sponsored by the U.S. National Science Foundation (NSF) and participating countries under the management of Joint Oceanographic Institutions (JOI), Inc. This work was funded by National Science Foundation grants OCE-9819053, OCE-0241940, and OCE-0326714 and by U.S. Scientific Support Program postcruise funding. We thank the officers, crew, scientists, and technicians who collected the physical property data set during Leg 210 aboard the *JOIDES Resolution* in the summer of 2003 and the SCREECH seismic reflection data set aboard the *Maurice Ewing* and the *Oceanus* in the summer of 2000. We gratefully acknowledge Dennis Harry and Andrew Goodliffe, who provided thoughtful and constructive reviews of this manuscript. We also thank Christian Berndt, who assisted with the software package Nucleus. This is Lamont-Doherty contribution number 6980.

REFERENCES

Bloomer, S.F., and Mayer, L.A., 1997. Core-log-seismic integration as a framework for determining the basin-wide significance of regional reflectors in the eastern equatorial Pacific. *Geophys. Res. Lett.,* 24(3):321–324. **doi:10.1029/96GL02076**

Boillot, G., Recq, M., Winterer, E.L., Meyer, A.W., Applegate, J., Baltuck, M., Bergen, J.A., Comas, M.C., Davies, T.A., Dunham, K., Evans, C.A., Girardeau, J., Goldberg, G., Haggerty, J., Jansa, L.F., Johnson, J.A., Kasahara, J., Loreau, J.P., Luna-Sierra, E., Moullade, M., Ogg, J., Sarti, M., Thurow, J., and Williamson, M., 1987. Tectonic denudation of the upper mantle along passive margins: a model based on drilling results (ODP Leg 103, western Galicia margin, Spain). *Tectonophysics,* 132(4):335–342. **doi:10.1016/0040-1951(87)90352-0**

Carlson, R.L., Gangi, A.F., and Snow, K.R., 1986. Empirical reflection travel time versus depth and velocity versus depth functions for the deep sea sediment column. *J. Geophys. Res.,* 91:8249–8266.

Chian, D., Louden, K.E., Minshull, T.A., and Whitmarsh, R.B., 1999. Deep structure of the ocean-continent transition in the southern Iberia Abyssal Plain from seismic refraction profiles: 1. Ocean Drilling Program (Legs 149 and 173) transect. *J. Geophys. Res.,* 104(B4):7443–7462. **doi:10.1029/1999JB900004**

Edwards, R.A., 1998. Integration of seismic reflection, physical properties, and downhole logging data. *In* Mascle, J., Lohmann, G.P., and Moullade, M. (Eds.), *Proc. ODP, Sci. Results,* 159: College Station, TX (Ocean Drilling Program), 225–240. **doi:10.2973/odp.proc.sr.159.028.1998**

Enachescu, M.E., 1992. Basement extension on the Newfoundland continental margin (Canadian east coast). *Basement Tecton.,* 7:227–256.

Fuchs, K.M., and Muller, G., 1971. Computation of synthetic seismograms with the reflectivity method and comparison with observations. *Geophys. J. R. Astron. Soc.,* 23:417–433.

Funck, T., Hopper, J.R., Larsen, H.C., Louden, K.E., Tucholke, B.E., and Holbrook, W.S., 2003. Crustal structure of the ocean–continent transition at Flemish Cap: seismic refraction results. *J. Geophys. Res.,* 108(B11):2531. **doi:10.1029/2003JB002434**

Hart, S.R., and Blusztajn, J., 2006. Age and geochemistry of the mafic sills, ODP Site 1276, Newfoundland margin. *Chem. Geol.,* 235(3–4):222–237. **doi:10.1016/j.chemgeo.2006.07.001**

Hopper, J.R., Funck, T., Tucholke, B.E., Larsen, H.C., Holbrook, W.S., Louden, K.E., Shillington, D., and Lau, H., 2004. Continental breakup and the onset of ultraslow seafloor spreading off Flemish Cap on the Newfoundland rifted margin. *Geology,* 32(1):93–96. **doi:10.1130/G19694.1**

IOC, IHO, and BODC, 2003. *GEBCO Digital Atlas—Centenary Edition (GEBCO-CE):* London (British Oceanographic Data Centre). [CD-ROM]

Jansa, L.F., Enos, P., Tucholke, B.E., Gradstein, F.M., and Sheridan, R.E., 1979. Mesozoic-Cenozoic sedimentary formations of the North American Basin, western North Atlantic. *In* Talwani, M., Hay, W., and Ryan, W.B.F. (Eds.), *Deep Drilling Results in the Atlantic Ocean: Continental Margins and Paleoenvironment.* Maurice Ewing Ser., 3:1–57.

Karner, G.D., and Shillington, D.J., 2005. Basalt sills of the U reflector, Newfoundland Basin: a serendipitous dating technique. *Geology,* 33(12):985–988. **doi:10.1130/G21971.1**

Keen, C.E., Boutilier, R., de Voogd, B., Mudford, B., and Enachescu, M.E., 1987. Crustal geometry and extensional models for the Grand Banks, eastern Canada: constraints from deep seismic reflection data. *In* Beaumont, C., and Tankard, A.J. (Eds.), *Sedimentary Basins and Basin-Forming Mechanisms.* CSPG Mem., 12:101–115.

Keen, C.E., and de Voogd, B., 1988. The continent-ocean boundary at the rifted margin off eastern Canada: new results from deep seismic reflection studies. *Tectonics,* 7:107–124.

Kennett, B.L.N., 1983. *Seismic Wave Propagation in a Stratified Media:* Cambridge (Cambridge Univ. Press).

Korenaga, J., Holbrook, W.S., Singh, S.C., and Minshull, T.A., 1997. Natural gas hydrates on the southeast U.S. margin: constraints from full waveform and travel time inversions of wide-angle seismic data. *J. Geophys. Res.,* 102(B7):15345–15366. **doi:10.1029/97JB00725**

Krawczyk, C.M., Reston, T.J., Beslier, M.-O., and Boillot, G., 1996. Evidence for detachment tectonics on the Iberia Abyssal Plain rifted margin. *In* Whitmarsh, R.B., Sawyer, D.S., Klaus, A., and Masson, D.G. (Eds.), *Proc. ODP, Sci. Results,* 149: College Station, TX (Ocean Drilling Program), 603–615. **doi:10.2973/odp.proc.sr.149.244.1996**

Lau, K.W.H., Louden, K.E., Deemer, S., Hall, J., Hopper, J.R., Tucholke, B.E., Holbrook, W.S., and Larsen, H.C., 2006a. Crustal structure across the Grand Banks—Newfoundland basin continental margin—II. Results from a seismic reflection profile. *Geophys. J. Int.,* 167(1):157–170. **doi:10.1111/j.1365-246X.2006.02989.x**

Lau, K.W.H., Louden, K.E., Funck, T., Tucholke, B.E., Holbrook, W.S., Hopper, J.R., and Larsen, H.C., 2006b. Crustal structure across the Grand Banks—Newfoundland basin continental margin—I. Results from a seismic refraction profile. *Geophys. J. Int.,* 167(1):127–156. **doi:10.1111/j.1365-246X.2006.02988.x**

Miller, K.G., and Tucholke, B.E., 1983. Development of Cenozoic abyssal circulation south of the Greenland-Scotland Ridge. *In* Bott, M.H.P., Saxov, S., Talwani, M., and Thiede, J. (Eds.), *Structure and Development of the Greenland-Scotland Ridge: New Methods and Concepts*. NATO Conf. Ser. IV, 8:549–589.

Minshull, T.A., and Singh, S.C., 1993. Shallow structure of oceanic crust in the western North Atlantic from seismic waveform inversion and modeling. *J. Geophys. Res.,* 98:1777–1792.

Norris, R.D., Klaus, A., and Kroon, D., 2001. Mid-Eocene deep water, the Late Palaeocene Thermal Maximum and continental slope mass wasting during the Cretaceous–Palaeogene impact. *In* Kroon, D., Norris, R.D., and Klaus, A. (Eds.), *Western North Atlantic Paleogene and Cretaceous Paleoceanography,* Geol. Soc. Spec. Publ., 183:23–48.

Sawyer, D.S., Whitmarsh, R.B., Klaus, A., et al., 1994. *Proc. ODP, Init. Repts.,* 149: College Station, TX (Ocean Drilling Program). **doi:10.2973/odp.proc.ir.149.1994**

Shillington, D.J., Holbrook, W.S., Tucholke, B.E., Hopper, J.R., Louden, K.E., Larsen, H.C., Van Avendonk, H.J.A., Deemer, S., and Hall, J., 2004. Data report: marine geophysical data on the Newfoundland nonvolcanic rifted margin around SCREECH transect 2. *In* Tucholke, B.E., Sibuet, J.-C., Klaus, A., et al., *Proc. ODP, Init. Repts.,* 210: College Station, TX (Ocean Drilling Program), 1–36. **doi:10.2973/odp.proc.ir.210.105.2004**

Shillington, D.J., Holbrook, W.S., Van Avendonk, H.J.A., Tucholke, B.E., Hopper, J.R., Louden, K.E., Larsen, H.C., and Nunes, G.T., 2006. Evidence for asymmetric nonvolcanic rifting and slow incipient oceanic accretion from seismic reflection data on the Newfoundland margin. *J. Geophys. Res.,* 111(B9):B09402. **doi:10.1029/2005JB003981**

Shipboard Scientific Party, 2004. Site 1276. *In* Tucholke, B.E., Sibuet, J.-C., Klaus, A., et al., *Proc. ODP, Init. Repts.,* 210: College Station, TX (Ocean Drilling Program), 1–358. **doi:10.2973/odp.proc.ir.210.103.2004**

Srivastava, S.P., Sibuet, J.-C., Cande, S., Roest, W.R., and Reid, I.D., 2000. Magnetic evidence for slow seafloor spreading during the formation of the Newfoundland and Iberian margins. *Earth Planet. Sci. Lett.,* 182(1):61–76. **doi:10.1016/S0012-821X(00)00231-4**

Sullivan, K.D., and Keen, C.E., 1978. On the nature of the crust in the vicinity of the southeast Newfoundland Ridge. *Can. J. Earth Sci.,* 15:1462–1471.

Tucholke, B.E., Austin, J.A., and Uchupi, E., 1989. Crustal structure and rift-drift evolution of the Newfoundland Basin. *In* Tankard, A.J., and Balkwell, H.R. (Eds.),

Extensional Tectonics and Stratigraphy of the North Atlantic Margins. AAPG Mem., 46:247–263.

Tucholke, B.E., and Mountain, G.S., 1979. Seismic stratigraphy, lithostratigraphy, and paleosedimentation patterns in the North American Basin. *In* Talwani, M., Hay, W., and Ryan, W.B.F. (Eds.), *Deep Drilling Results in the Atlantic Ocean: Continental Margins and Paleoenvironment.* Maurice Ewing Ser., 3:58–86.

Tucholke, B.E., Sawyer, D.S., and Sibuet, J.-C., 2007. Breakup of the Newfoundland-Iberia Rift. *In* Karner, G.D., Manatschal, G., and Pinheiro, L.M. (Eds.), *Imaging, Mapping, and Modeling Continental Lithosphere Extension and Breakup,* Geol. Soc., Spec. Publ., 282:9–46.

Van Avendonk, H.J.A., Holbrook, W.S., Nunes, G.T., Shillington, D.J., Tucholke, B.E., Louden, K.E., Larsen, H.C., and Hopper, J.R., 2006. Seismic velocity structure of the rifted margin of the eastern Grand Banks of Newfoundland, Canada. *J. Geophys. Res.,* 111(B11):B11404. **doi:10.1029/2005JB004156**

Whitmarsh, R.B., Beslier, M.-O., Wallace, P.J., et al., 1998. *Proc. ODP, Init. Repts.,* 173: College Station, TX (Ocean Drilling Program). **doi:10.2973/odp.proc.sr.173.2001**

Wold, C.N., 1994. Cenozoic sediment accumulation on drifts in the northern North Atlantic. *Paleoceanography,* 9(6):917–942. **doi:10.1029/94PA01438**

Zelt, C.A., and Smith, R.B., 1992. Seismic traveltime inversion for 2-D crustal velocity structure. *Geophys. J. Int.,* 108(1):16–34. **doi:10.1111/j.1365-246X.1992.tb00836.x**

Zühlsdorff, L., and Spiess, V., 2001. Modeling seismic reflection patterns from Ocean Drilling Program Leg 168 core density logs: insight into lateral variations in physical properties and sediment input at the eastern flank of the Juan de Fuca Ridge. *J. Geophys. Res.,* 106(B8):16119–16134. **doi:10.1029/2001JB900005**

Figure F1. Bathymetric maps of the Newfoundland margin based on the General Bathymetric Chart of the Oceans (IOC et al., 2003). Red lines = seismic reflection profiles from the SCREECH experiment. **A.** Entire SCREECH experiment with bathymetry contoured at 200-m intervals. **B.** Seismic lines around the ODP Leg 210 transect with bathymetry contoured at 200-m intervals.

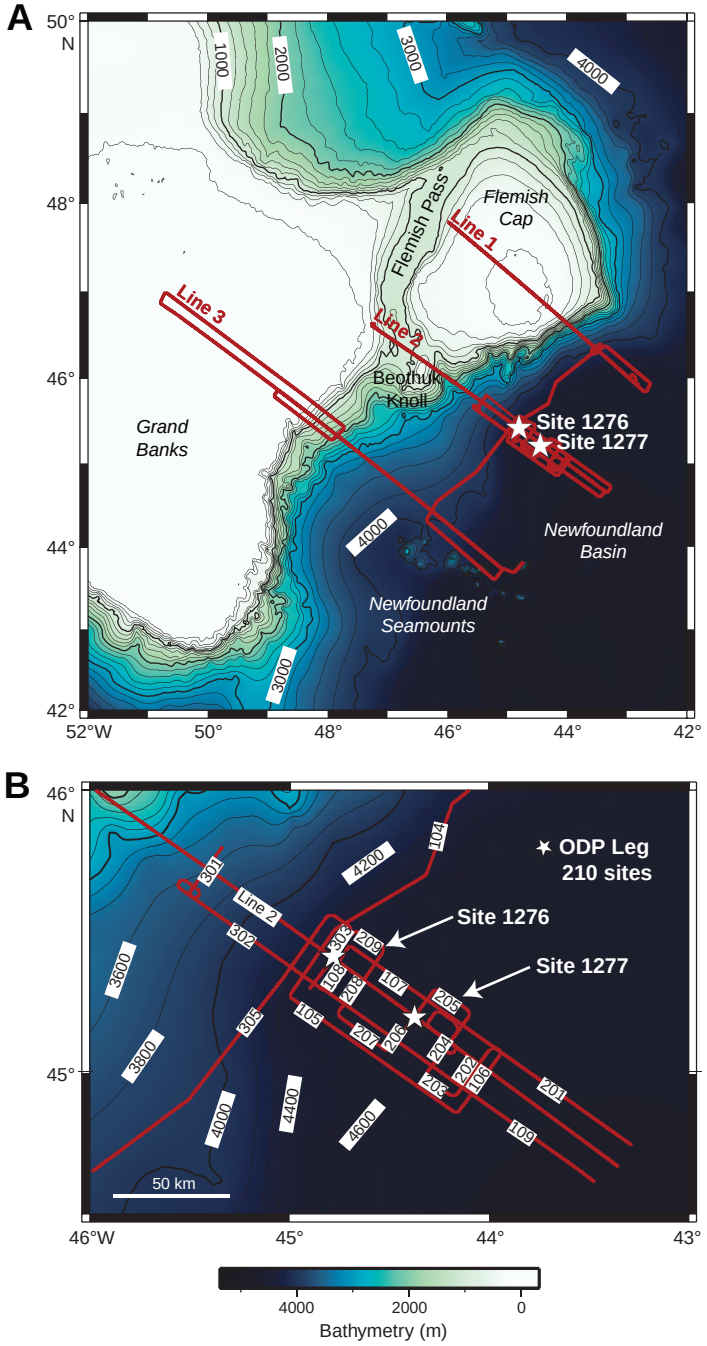

Figure F2. Prestack time migration of SCREECH Line 2, which crosses Sites 1276 and 1277 (Shillington et al., 2004). Note the continuity of seismic stratigraphic horizons (e.g., A^{U1}, A^{U2}, and U horizons) over much of the profile. **A.** Plot of the seaward two-thirds of the SCREECH Line 2. Locations of magnetic anomalies M3 and M0 are after Srivastava et al. (2000) and Shillington et al. (2004). Black box outlines region shown in B and C. **B.** SCREECH Line 2 covering transitional basement and Site 1276. Few basement features can be observed beneath the strong U reflection and other reflections in the lowermost sedimentary section. **C.** Same profile as B, with interpretations of the A^{U1}, A^{U2} (after **Tucholke and Sibuet;** this volume), and U reflections, indicated with purple, red, and blue dashed lines, respectively.

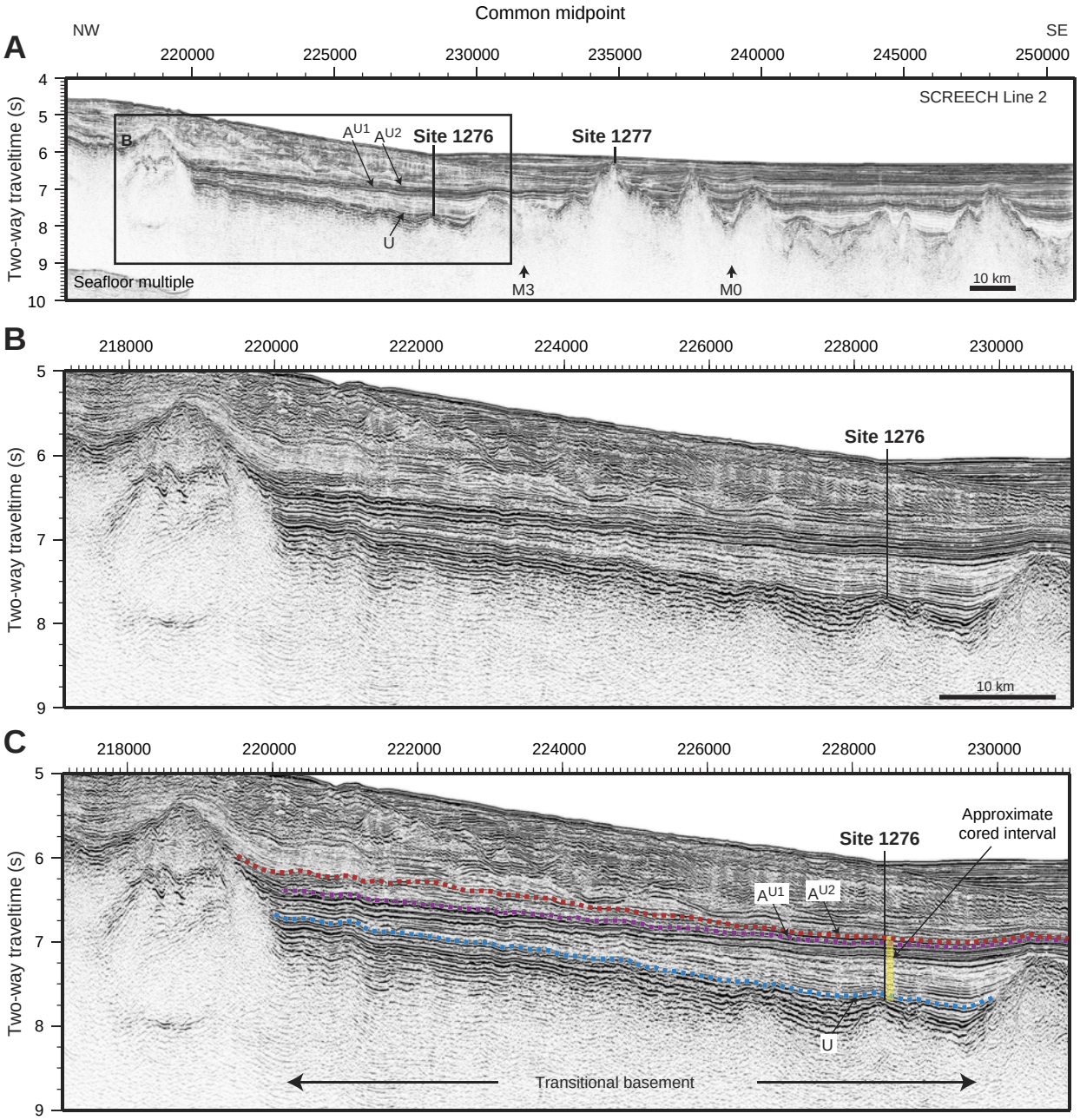

Figure F3. Laboratory measurements of vertical (*z*) and horizontal (*x*) *P*-wave velocity and of density made during Leg 210 at Site 1276 (Shipboard Scientific Party, 2004). Graphs do not cover the full range of measured values; complete data set is archived in the Janus database (**www-odp.tamu.edu/database**). Colored lines = averages calculated over a moving window of 20 m to illustrate downhole trends for display purposes only. Lithologic units from Shipboard Scientific Party (2004). Vertical *P*-wave velocities and densities were used to calculate synthetic seismograms in Figures **F9,** p. 28, and **F10,** p. 29.

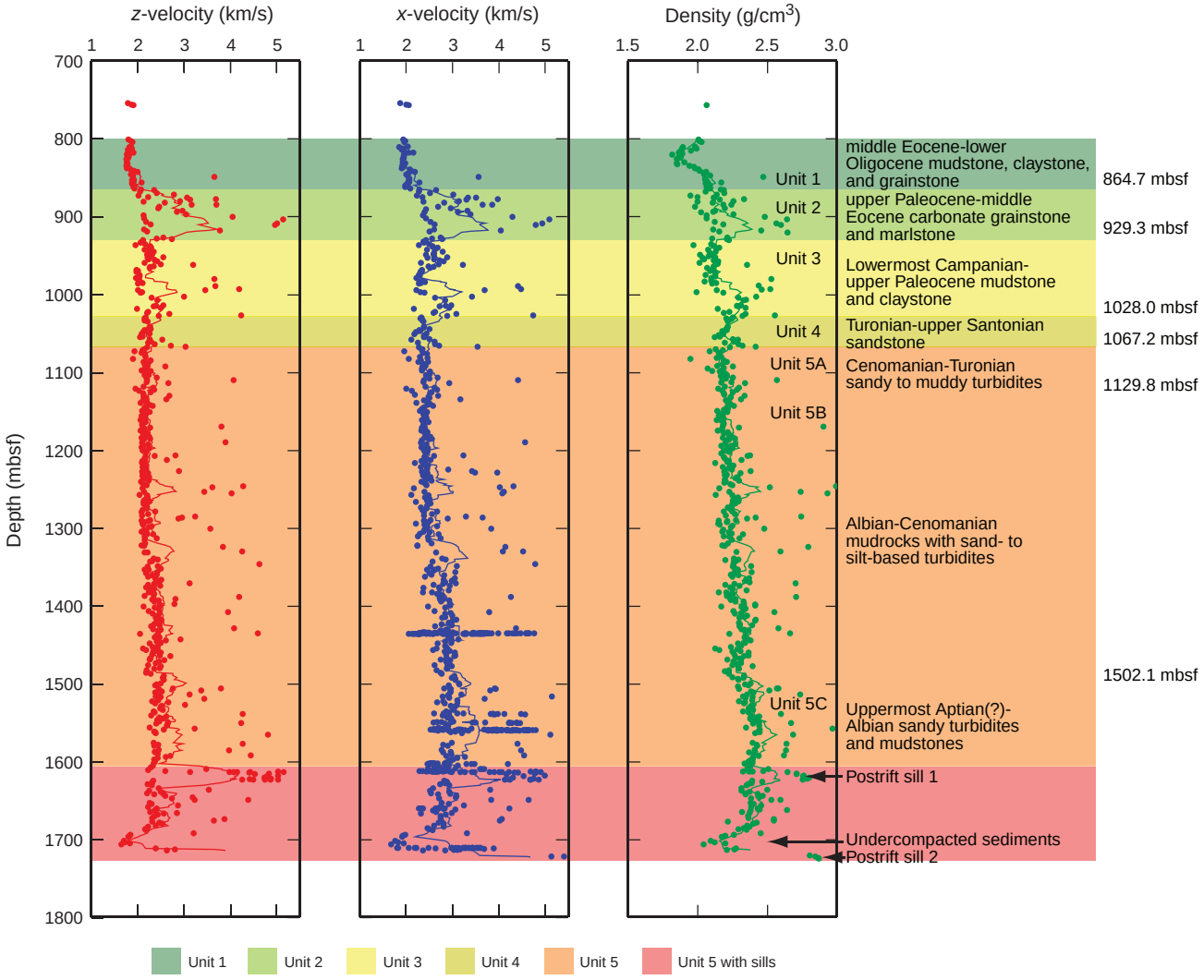

Figure F4. Three scenarios for processing physical property measurements to address possible sampling biases. Graphic lithology is based on shipboard core description from 1242 to 1249 mbsf (Unit 5) (Shipboard Scientific Party, 2004). Blue triangles = measurements of vertical *P*-wave velocity at discrete locations. Note that two of these measurements were taken from thin (<5 cm) lithologic intervals with velocities that are not representative of the surrounding 2 m of core. This has potentially important consequences for synthetic seismograms derived from these measurements. We explore the effects of possible biases in sample selection in the following three ways: Scenario 1 = create synthetics from measured velocities and densities without modifying apparent bed thickness implied by spacing between measurements, Scenario 2 = remove measurements that are >3 km/s in lithologic Unit 5 if measurement was made on sample from a thin (<1 m) lithologic layer, and Scenario 3 = modify range of depths over which measurements of velocity >3 km/s is extrapolated so that it is similar to the thickness of the lithologic interval from which it was taken.

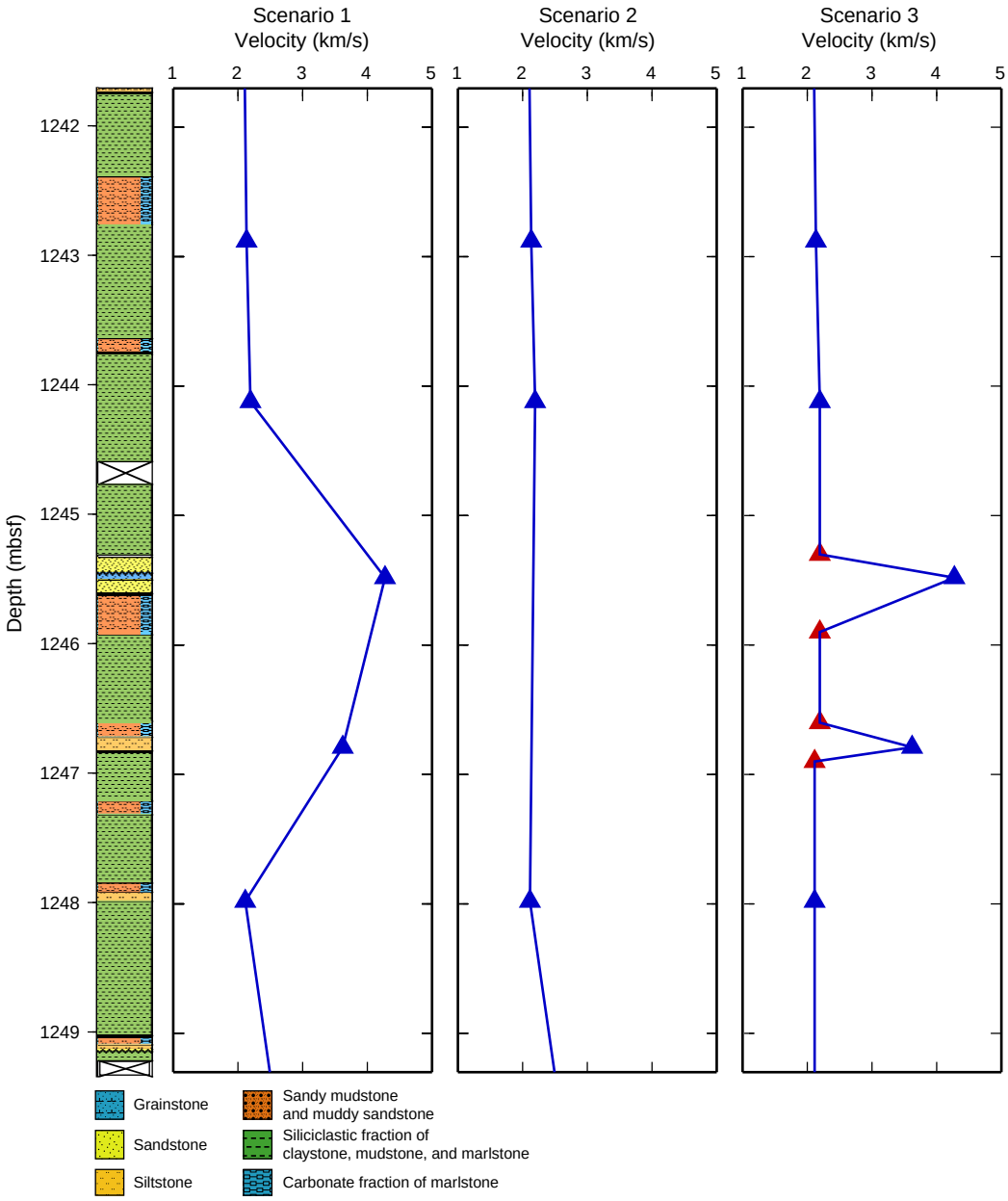

Figure F5. Creation of earth model used to calculated synthetic seismograms and its representation in the resulting velocity function. Layers are hand-selected by the user to group together similar velocities. Velocities and densities assigned to layers are averages of the interpolated input velocity function. As a result, actual velocities and densities assigned to each layer are neither as high nor as low as original data points.

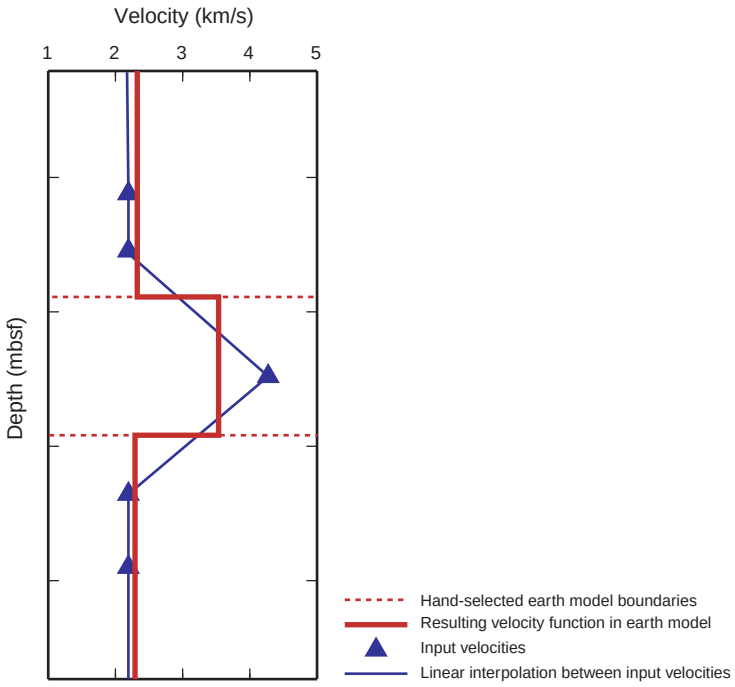

Figure F6. Velocity functions used to calculate reflection coefficient series for each of the three physical property processing scenarios described in text and illustrated in Figure F4, p. 23. Black lines = velocity functions, blue dots = laboratory measurements of vertical (*z*) *P*-wave velocities. In Scenario 1, all measured velocities from physical properties are used to pick layers and calculate reflection coefficient series. In Scenario 2, velocities >3 km/s from thin (<1 m) lithologic intervals are removed where they were measured in Unit 5 above the upper sill (1067–1612 mbsf). In Scenario 3, the thickness spanned by high-velocity laboratory measurements is modified to represent the thickness of the corresponding lithology in core descriptions.

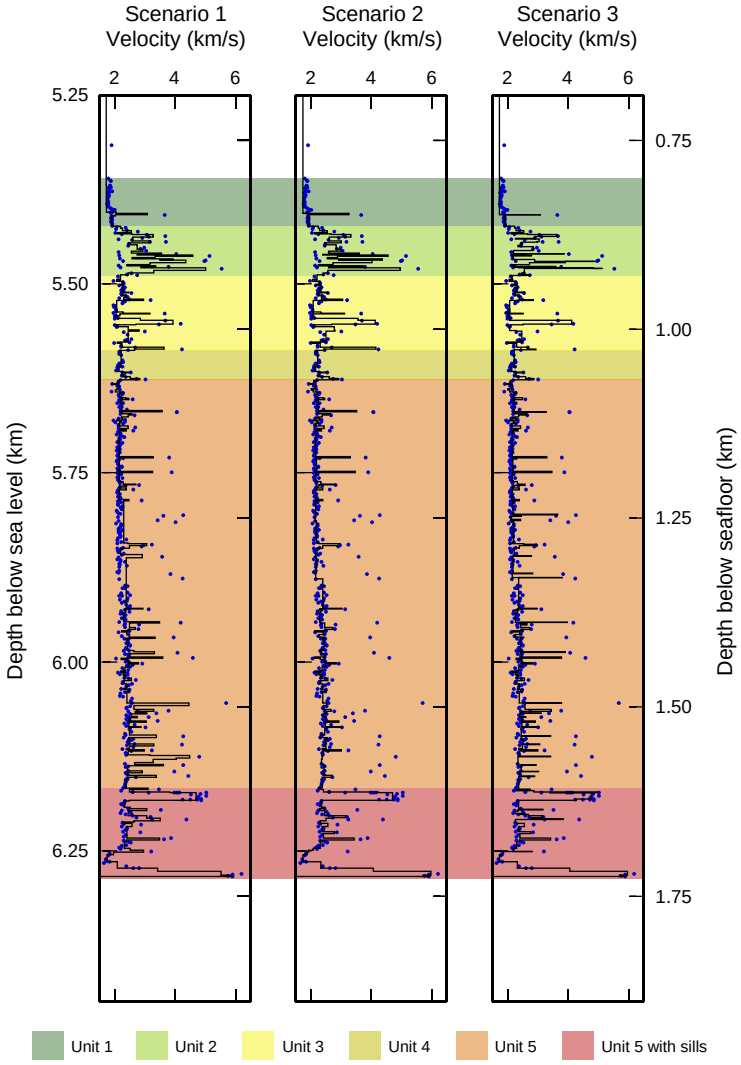

Figure F7. Estimates of seismic source wavelet derived in three ways: red line = modeled from air gun source configuration of the *Maurice Ewing* using the commercial software package Nucleus; green line = extracted from SCREECH MCS data by deconvolving the first seabed multiple with the first arrival, as described by Korenaga et al. (1997); and blue line = a trace extracted from SCREECH prestack seismic data near Site 1276. Amplitudes of each trace have been normalized so that the maximum positive amplitude = 1. CMP = common midpoint.

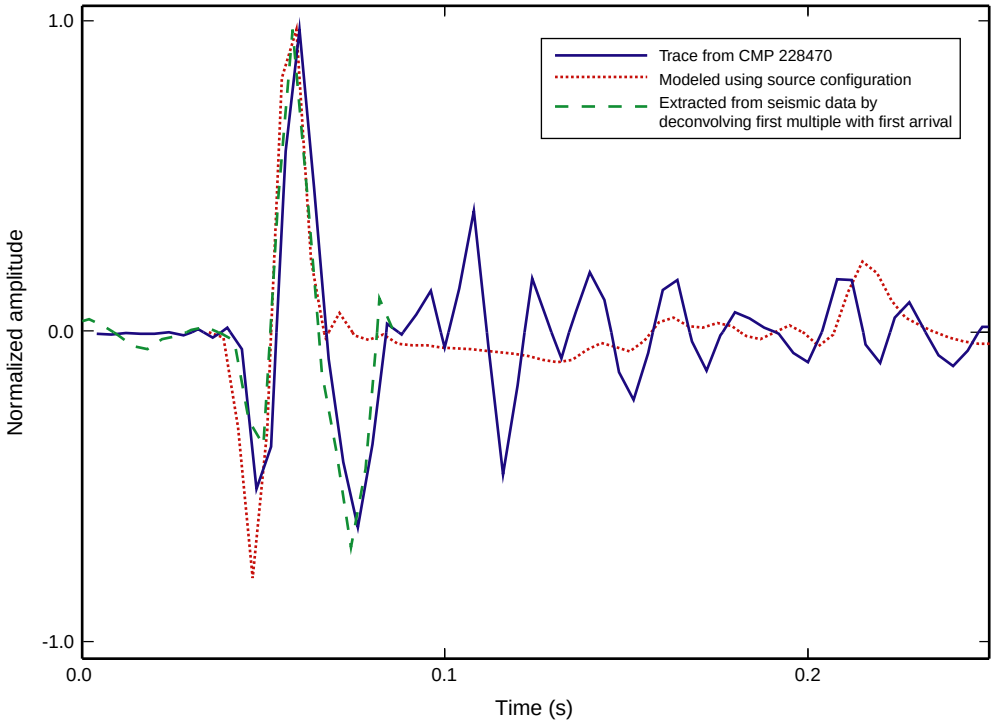

Figure F8. Velocity modeling of multichannel seismic (MCS) reflection data to determine velocities in upper 800 m of sedimentary section at Site 1276, where no cores or downhole logs were obtained. **A.** Section of a prestack time migration of SCREECH Line 2 together with a common midpoint (CMP) gather close to Site 1276. Colored lines indicate picks used for velocity modeling described in text. **B.** 1-D velocity-depth function derived from velocity modeling (red line) plotted together with laboratory measurements of vertical *P*-wave velocity from Site 1276 (blue dots) and a moving average of these measurements calculated with 100-m window (blue line) for display purposes. Velocities derived from velocity modeling were used above the first laboratory measurement (<800 mbsf) to create synthetic seismograms.

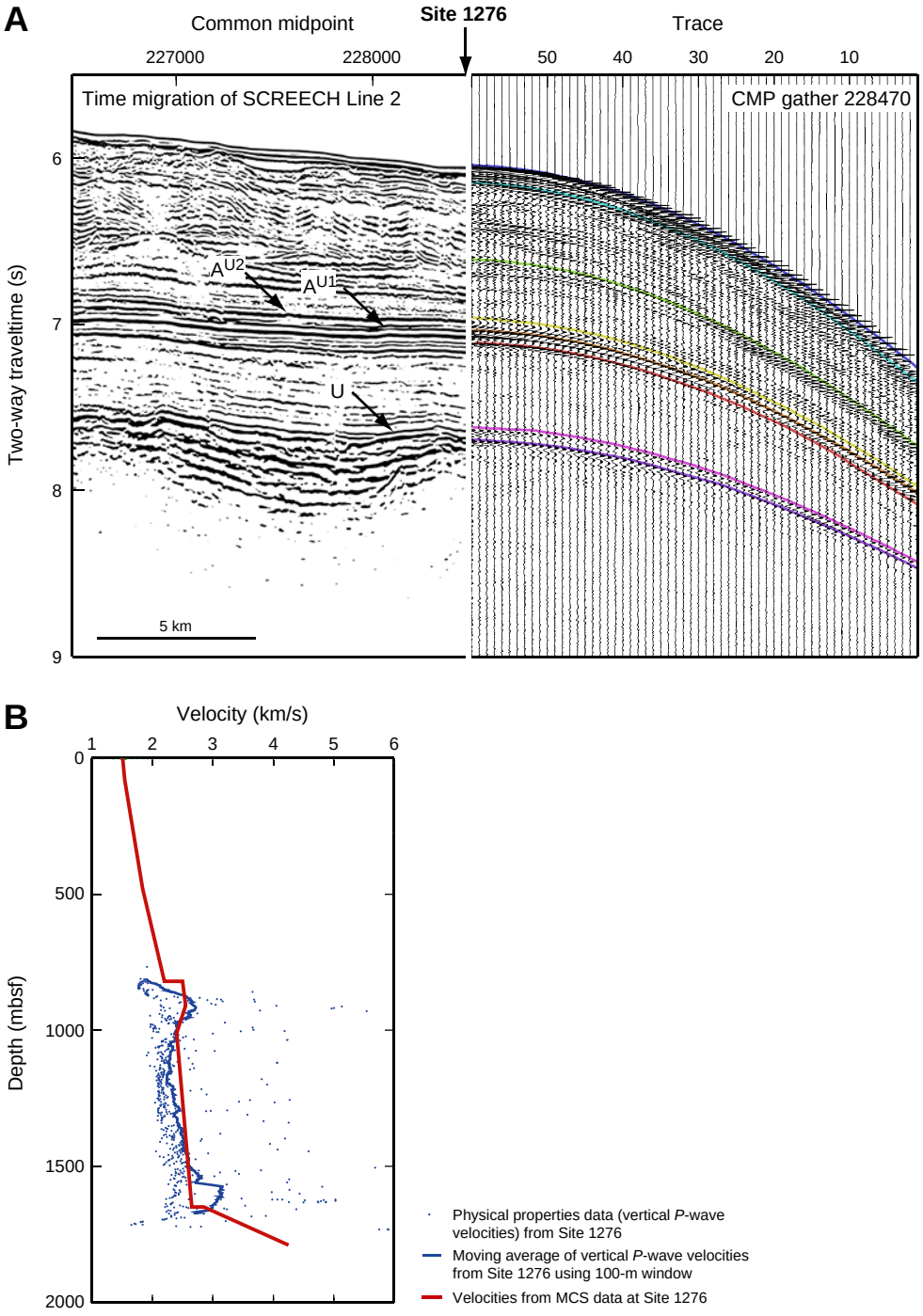

Figure F9. A–C. Synthetic seismograms calculated using the three different scenarios for processing physical property data illustrated in Figures F4, p. 23, and F6, p. 25. For each scenario, the velocity function used is shown together with lithologic units (color coded by unit), and the synthetic seismogram is plotted immediately to the right. Twenty wiggle traces and 200 variable density traces from SCREECH Line 2 MCS data at Site 1276 are plotted for comparison; wiggle traces best represent observed amplitudes at the drill site. Synthetics generated for all three scenarios recover the first-order features observed in the MCS reflection data. Top of green box = top of cored interval (800 mbsf); in all cases this level is converted to TWT using velocities from modeling of MCS data between the seafloor and 800 mbsf. Reflections that appear in synthetic seismograms after the last sample are caused by interbed multiples and other effects included in the reflectivity method.

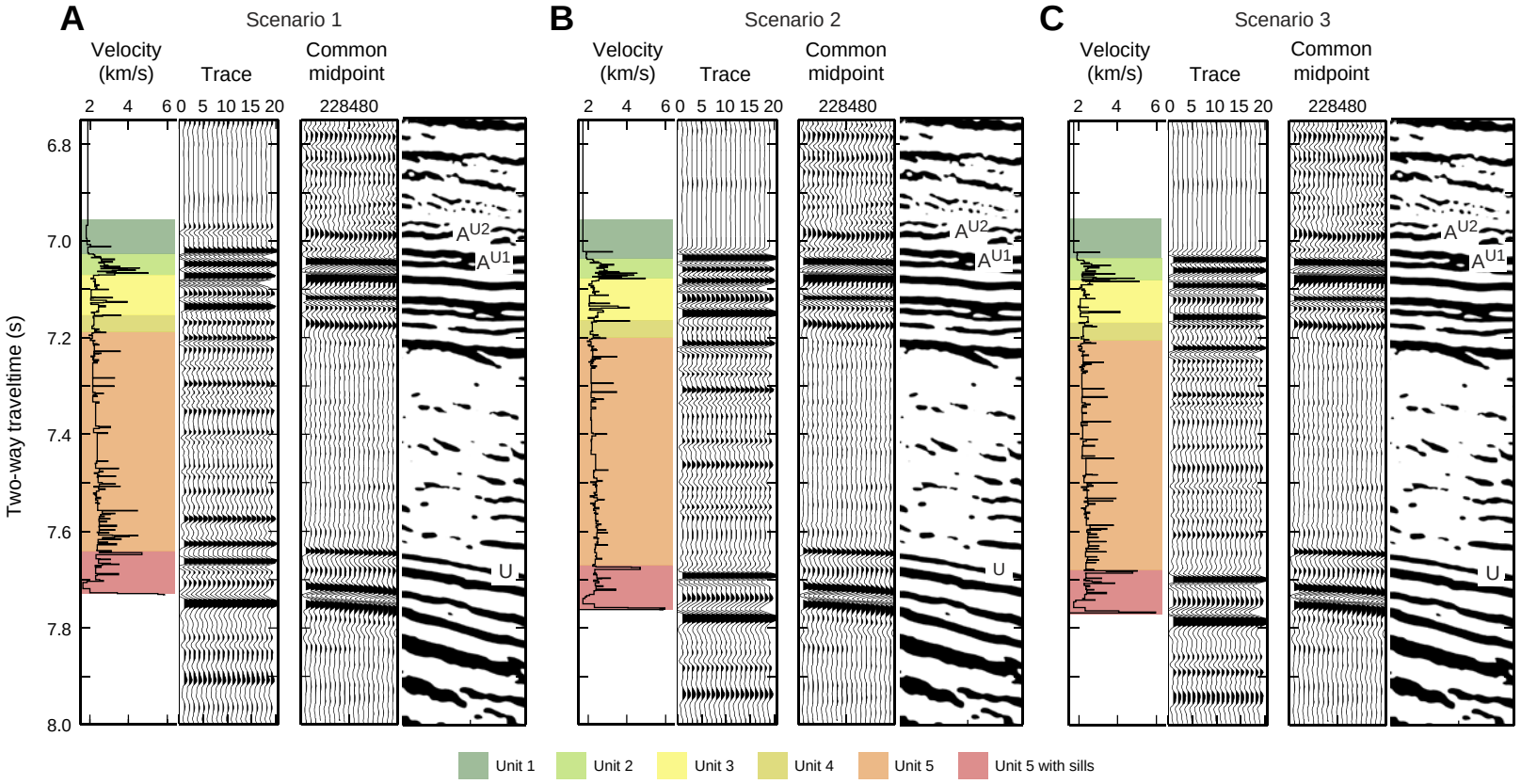

Figure F10. Three alternative correlations between synthetic and observed data using the synthetic seismogram from Scenario 3 (Fig. F9C, p. 28). For each interpretation, the velocity function used is shown together with lithologic units (color coded by unit), and the synthetic seismogram is plotted immediately to the right. Twenty wiggle traces and 200 variable density traces from SCREECH Line 2 MCS data at Site 1276 are plotted for comparison; wiggle traces best represent observed amplitudes at the drill site. Synthetics generated for all three interpretations recover the first-order features observed in the MCS reflection data. Red dashed lines = interpreted correlations between synthetic and observed data. **A.** Interpretation 1: the Unit 1/2 boundary correlates with the A^{U1} reflection (~7.02 s), and the Unit 4/5 boundary correlates to the apparent seismic unconformity at ~7.19 s in reflection data. **B.** Interpretation 2: the Unit 1/2 boundary corresponds to the A^{U2} reflection (~6.96 s), and the Unit 4/5 boundary corresponds to the reflection at ~7.16 s. **C.** Interpretation 3: the Unit 1/2 boundary corresponds to the reflection beneath the A^{U1} reflection (~7.04 s), and the Unit 4/5 boundary corresponds to the reflection at ~7.22 s. See text for discussion of each interpretation.

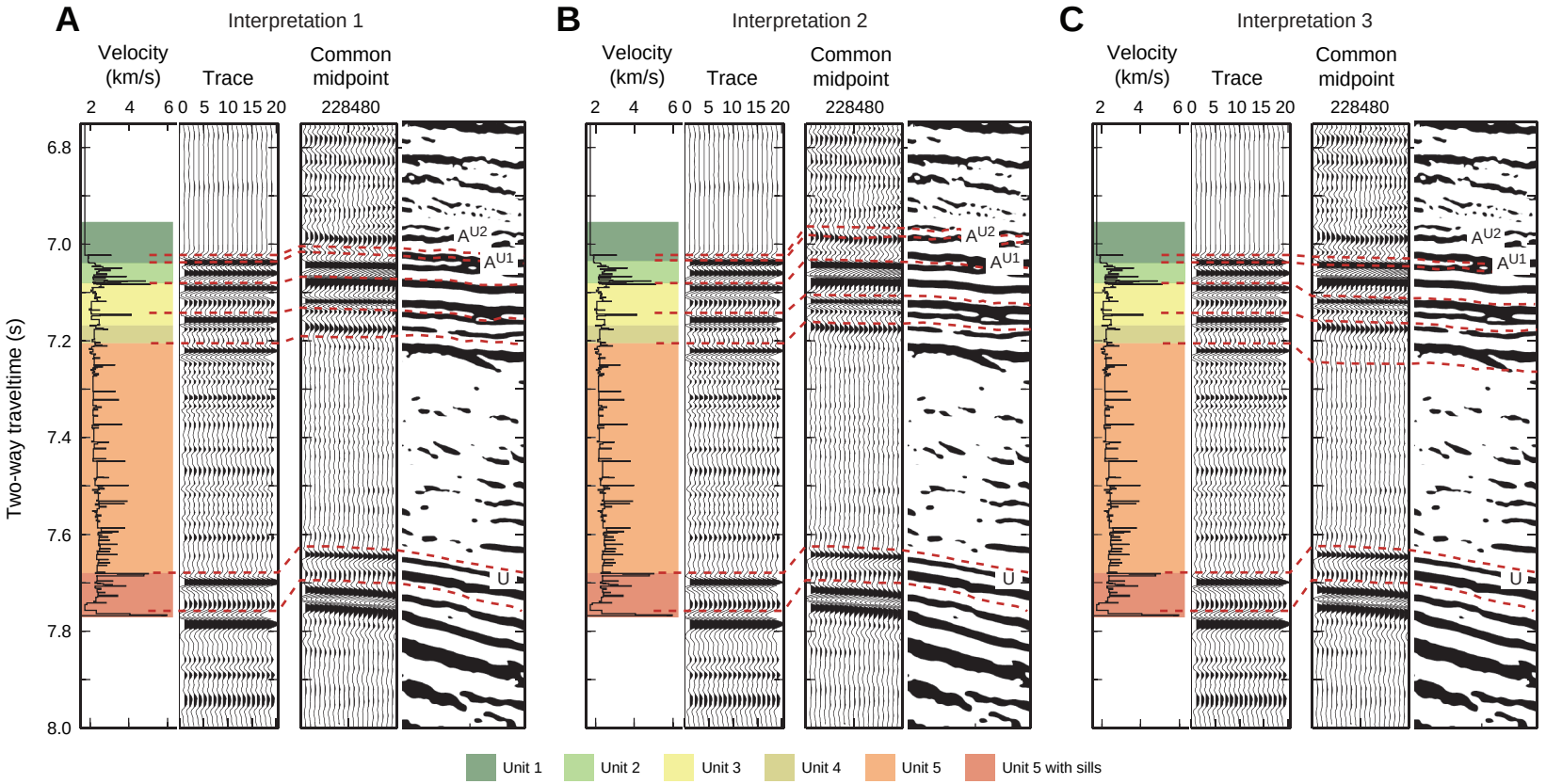

Figure F11. Comparison of average velocities above and below the lithologic Unit 1/2 boundary at 865 mbsf, as estimated by modeling of MCS data and implied by each of the interpretations shown in Figure F10, p. 29. See Table T1, p. 32 for times associated with 865 mbsf for each interpretation and more details on calculated average velocities and differences from average MCS velocities. Note that average velocity implied by Interpretation 2 closely matches average MCS velocity above 865 mbsf but is much lower than average MCS velocity below this level. Average velocity implied by Interpretation 3 is much lower than average MCS velocity above 865 mbsf, but average velocity in the deeper section is higher than MCS velocity. Average velocities implied by Interpretation 1 are relatively close to average MCS velocities both below and above 865 mbsf.

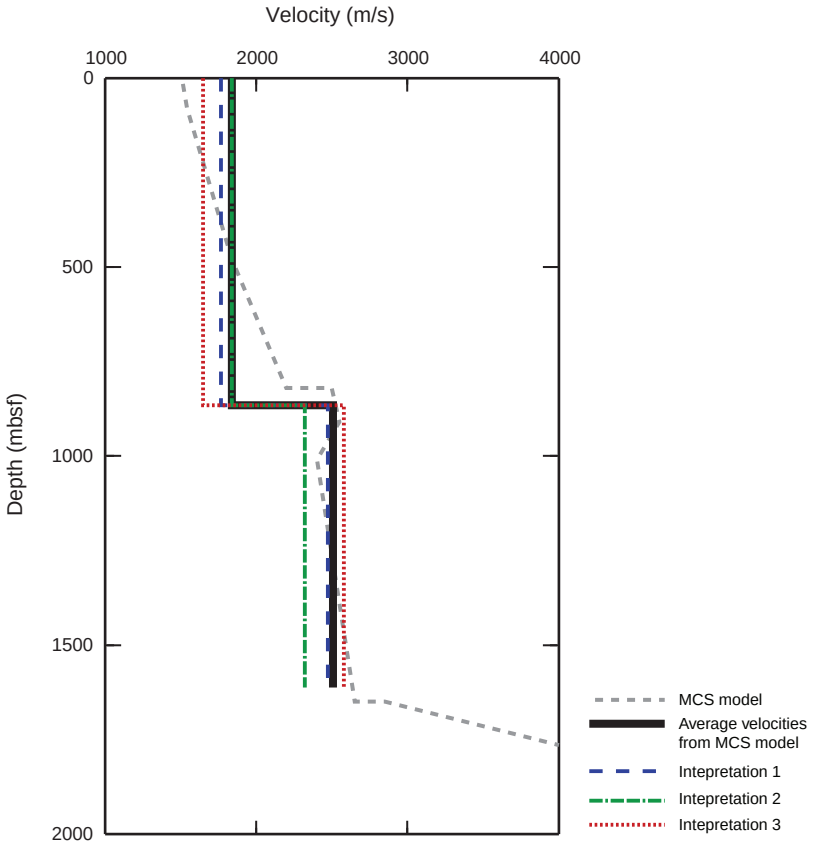

Figure F12. Interpretation of seismic horizons observed on a section of SCREECH Line 2 based on Interpretation 1 (Fig. **F10A,** p. 29), which uses the synthetic seismogram calculated from physical properties processing Scenario 3 (Fig. **F9C,** p. 28). The common midpoint panel shows interpreted segment of SCREECH Line 2 multichannel seismic (MCS) data (Shillington et al., 2004) that crosses Site 1276 (indicated with an arrow at the base of the plot). The MCS panel shows individual traces from coincident MCS reflection data. The synthetic seismogram has been shifted and stretched based on synthetic seismic correlations in Interpretation 1 (Fig. **F10A,** p. 29). The velocity function was used for synthetic seismogram generation together with lithologic units, ages, and dominant lithologies. Red dotted line = final interpretation of the A^U reflection (after **Tucholke and Sibuet,** this volume) described in the text.

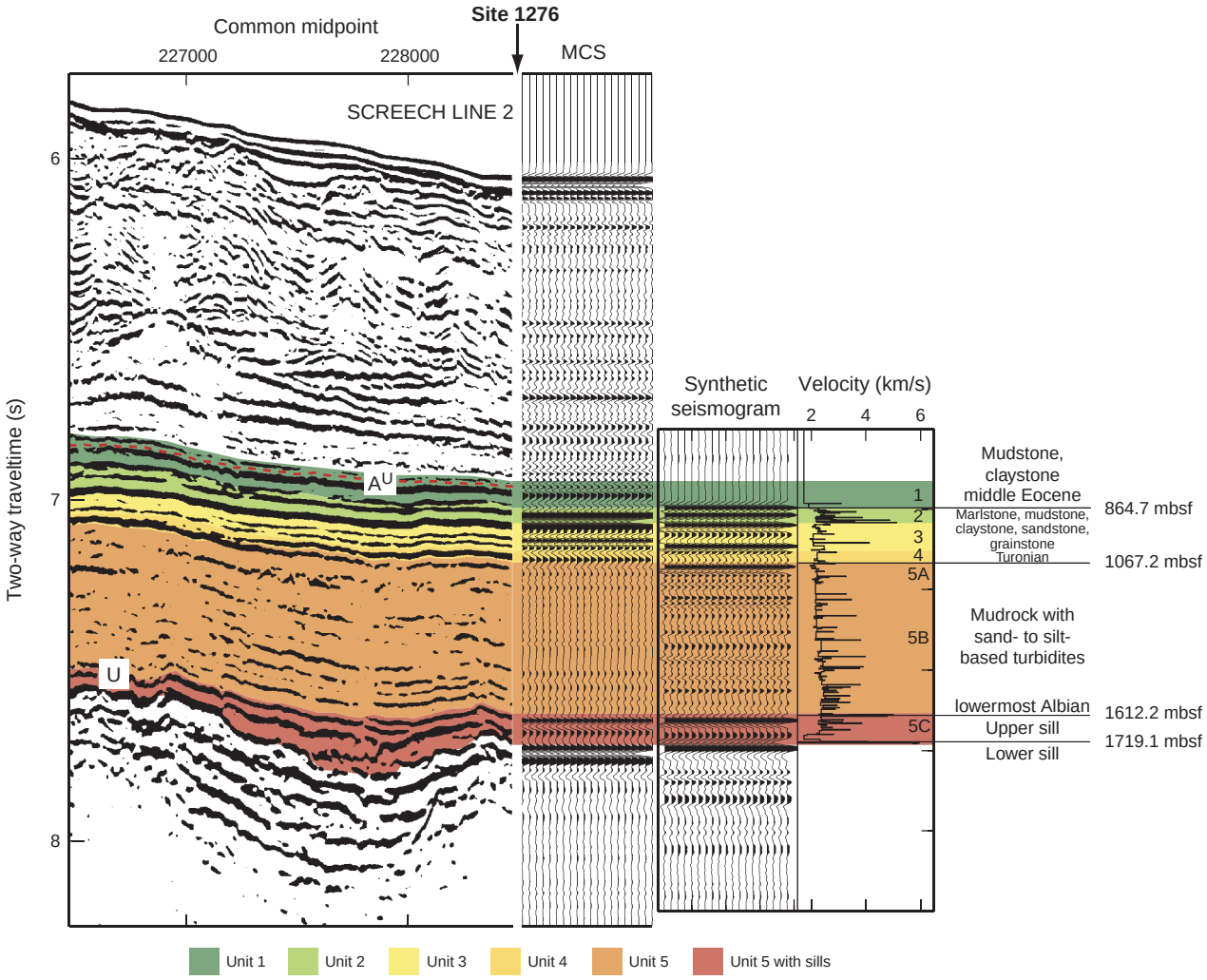

Table T1. Two-way traveltimes (TWTs) for the seafloor, 865 mbsf, and the upper sill for each of the interpretations shown in Figure **F10,** p. 29.

	MCS model	Interpretation 1	Interpretation 2	Interpretation 3
TWT of synthetic reflection linked to 865 mbsf		7.02 s	6.98 s	7.045 s
TWT between seafloor and reflection linked to 865 mbsf		0.98 s	0.94 s	1.05 s
Average velocity between seafloor and 865 mbsf	1839 m/s	1765 m/s	1840 m/s	1648 m/s
Difference between MCS model and inferred velocity for the layer between seafloor and 865 mbsf		74 m/s	1 m/s	191 m/s
TWT of synthetic reflection linked to upper sill		7.625 s	7.625 s	7.625 s
TWT synthetic reflection linked to 865 mbsf and reflection linked to upper sill		0.605 s	0.645 s	0.58 s
Average velocity between 865 mbsf and U reflection/upper sill	2508 m/s	2473 m/s	2319 m/s	2579 m/s
Difference between MCS model and inferred velocity for the layer between 865 mbsf and upper sill		35 m/s	189 m/s	71 m/s

Notes: Average velocities for the layers defined by these horizons are calculated from multichannel seismic (MCS) data and implied by each of the interpretations. Differences between velocities are derived from the interpretations and those from MCS data.

CHAPTER NOTE

N1. Wood, A.S., Gardin, S., and Wise, S.W., Jr., submitted. Age constraint and interpretations of a disconformity in the Newfoundland-Iberia rift basin, Ocean Drilling Program Leg 210. *Rev. Micropaleontol.*

*Dates reflect file corrections or revisions.